

Effects of Wind, Waves, and Currents on Icebergs and Surface Floats in the Labrador Sea: A Modeling Study

by

© *Jamseena Parayil*

A thesis submitted to the
School of Graduate Studies
in partial fulfilment of the
requirements for the degree of
Master of *Physical Oceanography*

Department of *Physics and Physical Oceanography*
Memorial University of Newfoundland

November 2022

St. John's

Newfoundland

Abstract

Icebergs are major indicators of climate change. In Newfoundland, icebergs attract tourists while simultaneously posing a threat to ships and offshore oil platforms. Research is carried out on a model study of the dynamics of icebergs and surface floats in the Labrador Sea. In this study, the iceberg model is forced with data of wind above the ocean surface, surface waves and ocean currents. The wind and surface wave characteristics are acquired from the hourly ECMWF reanalysis (ERA5), while the ocean current, sea-surface height and sea surface temperature data are from MERCATOR Ocean International daily reanalysis for the year 2008. In the Labrador Sea, for smaller icebergs the primary balance is between the air and water drag, while for larger icebergs it is between three forces: the air and water drag and the combined Coriolis and pressure force. Floats are primarily driven by the Ekman component of surface velocity. Storms passing over the Labrador Sea cause significant variability in the movements of icebergs and floats.

Acknowledgements

It is my immense pleasure to express my sincere gratitude to my supervisor, Dr. Entcho Demirov, who inspired me throughout my program. I sincerely thank my esteemed and worthy project guide for his valuable guidance in carrying out this work under his effective encouragement, motivation, and cooperation. Next, I would like to thank Dr. Yakov D. Afanasyev who has supported me and offered encouragement throughout this period.

I am immensely pleased to state my deep sense of gratitude to my family and friends for their support, especially my husband, Muhammed Asif.

Finally, I would like to thank the Department of Physics and Physical Oceanography for the access they have provided to their facilities and the Ocean Frontier Institute for the financial support I have been granted.

Contents

Abstract	ii
Acknowledgements	iii
List of Tables	vi
List of Figures	vii
1 Introduction	1
1.1 Fate of the Titanic	1
1.2 The origin of icebergs	4
1.2.1 Greenland Ice Sheet	7
1.2.2 Antarctic Ice Sheet	8
1.3 Iceberg distribution	10
1.3.1 Methods of iceberg observation	10
1.3.2 Northern Hemisphere	13
1.3.3 Southern Hemisphere	14
1.4 Icebergs' impacts	17
1.4.1 Safety of the maritime and offshore industry	17

1.4.2	Icebergs as a freshwater source	20
1.5	Physics of icebergs	22
1.5.1	Basic forces driving iceberg motion	22
1.5.2	Iceberg thermodynamics	25
1.6	Iceberg modelling	28
1.7	Motivation of the study	30
2	Model, Data and Methodology	31
2.1	Data sets	31
2.2	Model and Methodology	32
2.2.1	Time stepping	38
3	Results	39
3.1	Surface floats	39
3.2	Icebergs	43
4	Conclusions	53
	Bibliography	55

List of Tables

2.1 The iceberg categories. 34

List of Figures

1.1	Map of Greenland and the Labrador Sea showing the dominant paths of icebergs with permission of Grant. R. Bigg and acknowledgement to John Wiley and Sons	2
1.2	The total number of icebergs in the North-West Atlantic with a diameter of > 5 m crossed the latitude of 48° N for the year 1900 - 2014, with permission of Grant. R. Bigg	4
1.3	Chart for sea-level pressure and temperature on 15 April 1912 at 0000 GMT, with permission of Grant. R. Bigg and acknowledgement to G. P. Compo, J. S. Whitaker, P. D. Sardeshmukh([9])	5
1.4	Distribution of glaciers in the World Ocean ([11])	6
1.5	Names of the main glaciers of Greenland, (https://www.nasa.gov/mission_pages/icebridge/3.html/)	7
1.6	Rate of change of the mass of Greenland's glaciers with acknowledgement to Dr Tom Slater, (https://www.antarcticglaciers.org/glaciers-and-climate/changing-greenland-ice-sheet/greenland-ice-sheet-mass-balance/)	9
1.7	The North Atlantic mean iceberg zone, with permission of Grant. R. Bigg and acknowledgement to the International Ice Patrol	13

1.8	The figure represents the mean seasonal variation in iceberg number from the year 1900 to 2012, at 48° N, and this line extends from Newfoundland to 40° W, with permission of Grant. R. Bigg and acknowledgement to the International Ice Patrol	15
1.9	The number and mass of icebergs with a size > 18 km. The data is from the year 1979 to 2003, with permission of Grant. R. Bigg and acknowledgement to John Wiley and Sons.	16
1.10	Captain Cook obtaining fresh water from an iceberg, with permission of Grant. R. Bigg and acknowledgement to Captain Cook	20
1.11	Schematic representation of the forces responsible for the movement of icebergs	23
2.1	Map of the computational domain and circulation in the subpolar North Atlantic. The arrows show major currents in the subpolar gyre, including the North Atlantic Current (NAC), the Eastern Greenland Current (EGC), the Western Greenland Current (WGC), and the Labrador Current (LC).	32
2.2	Annual mean surface forcing used in the iceberg model (a) surface wind stress; (b) direction and mean height of surface waves; (c) sea surface temperature (contour interval 1° C), (d) sea surface height (contour interval 2 cm).	33

3.1	Annual mean and contours of standard deviation of (a) ocean surface velocity (contour interval 0.05 cm/s); (b) geostrophic velocity (contour interval 0.05 m/s) , (b) Ekman velocity (contour interval 0.05 m/s), and (d) Stokes velocity (contour interval 0.01 m/s).	41
3.2	Surface float trajectories (a) and velocity components (b). Trajectories are colored according to the annual mean sea surface temperature at the point of release: $t > 16^{\circ}C$ (red), $3^{\circ}C < t < 16^{\circ}C$ (green) and $t < 3^{\circ}C$ (blue). Quasigeostrophic (red line), Ekman (green line) and Stokes (blue line) components of velocity are averaged over the entire ensemble of floats.	43
3.3	Trajectories of icebergs of different mass: categories 3 (a), 4 (b), 5 (c), 7 (d), 9 (e) and 10 (f) (Table 2.1)	45
3.4	The magnitude of forces applied on icebergs of different mass during the first 120 days of their journey: categories 3 (a), 4 (b), 5 (c), 7 (d), 9 (e) and 10 (f) (Table 2.1)	49
3.5	Vector diagrams of forces for icebergs of different mas during a storm event: categories 4 (a), 5 (b), 9 (c) and 10 (d) (Table 2.1).	50
3.6	Vector diagrams of air, water and iceberg velocity for icebergs of different mass during a storm event: categories 4 (a), 5 (b), 9 (c) and 10 (d) (Table 2.1).	51
3.7	Intensity of melting along the iceberg paths: categories 3 (a), 4 (b), 5 (c), 7 (d), 9 (e) and 10 (f) (Table 2.1)	52

Chapter 1

Introduction

1.1 Fate of the Titanic

The Royal Mail Ship (RMS) Titanic started its journey from Southampton, England, to New York City on the 10th of April 1912 with 2200 people aboard. On the 14th of April 1912, at 11:40 pm, the vessel hit an iceberg and sank in the western North Atlantic, causing the deaths of 1512 people. The iceberg that caused the accident, which is often called the "Titanic iceberg", hit the ship at $41^{\circ}47'$ N, $49^{\circ}55'$ n ('+' in Figure 1.1). The motion of the Titanic iceberg in the North-west Atlantic was determined by the anti-clockwise direction of the ocean currents that carried it around the Labrador Sea and Baffin Bay towards 40° N (Figure 1.1). Most of the icebergs in this area form along the western coast of Greenland.

According to recent coupled ocean iceberg models, the calving location of the Titanic iceberg was southwest of the South Dome. The South Dome is the part of the Greenland Ice Sheet (GrIS) with a maximum accumulation rate (~ 0.55 m/yr).

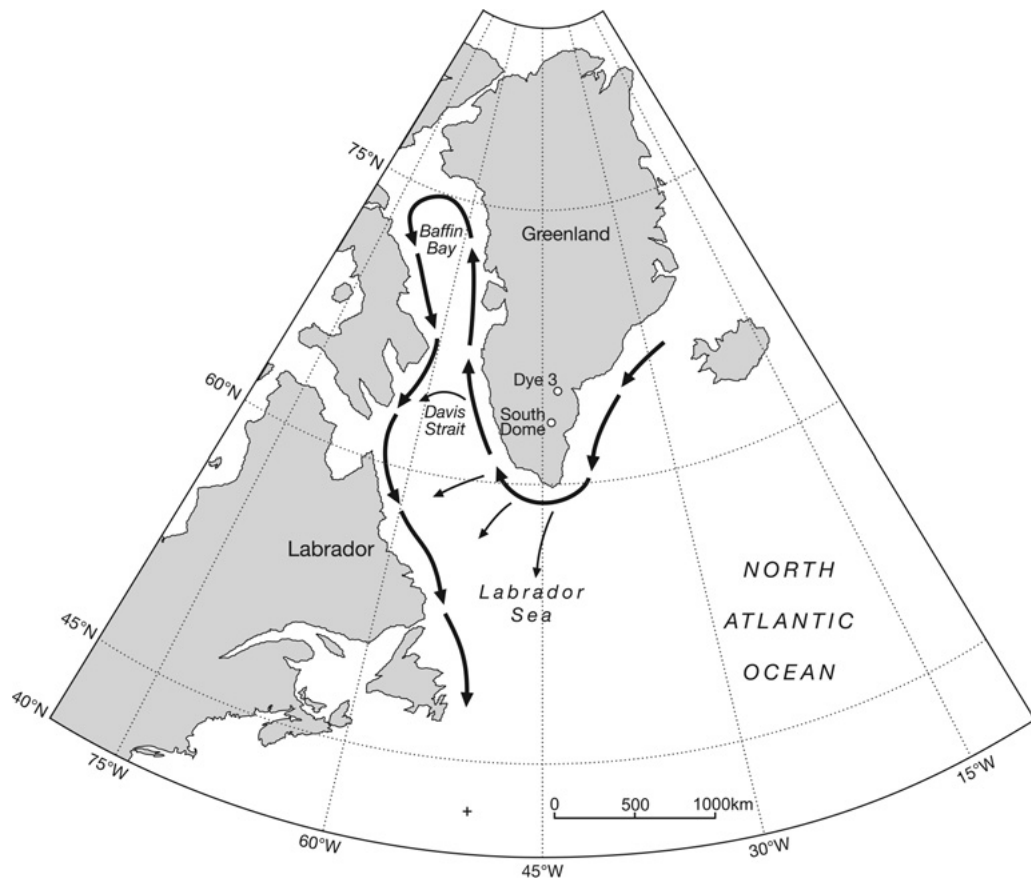


Figure 1.1: Map of Greenland and the Labrador Sea showing the dominant paths of icebergs with permission of Grant. R. Bigg and acknowledgement to John Wiley and Sons

It lies on the edge of the North Atlantic storm belt, producing high amounts of precipitation and ice accumulation. This region has the highest summer melt rate compared to other regions due to its proximity to relatively warm seas and landmasses. The glaciers consolidated earlier than 1400AD. The Titanic iceberg's ice age has been estimated to be between 1000 and 100,000 years old.

Presently, the International Ice Patrol (IIP) and the US Coast Guard monitor icebergs in the Northwest Atlantic Ocean for the safety of shipping vessels. Figure 1.2 shows the observed monthly number of icebergs greater than 5 m in dimension passing south of 48° N from 1900 to 2004. In 1912, the number of icebergs crossing 48° N was 1038, and 395 were present in April ([5]). The coupled ocean iceberg model suggests that the Titanic iceberg calved in the late summer to fall of 1911. The initial size of the iceberg was 15-31 m high, 122 m long, and 90 -185 m deep. The approximate mass was 1.0 tons (1000 kg).

Figure 1.3 represents the sea-level pressure and air temperature. March and April of 1912 were anomalously cold over eastern Canada and the western North Atlantic from 35° to 55° N. The air temperature was more than 2°C lower than the 1981 - 2010 mean. In early April, a center of high surface pressure dominated the atmospheric circulation of the North Atlantic. The cold air over eastern Canada was transported to the ocean by NW wind. These conditions supported the southward ice transport in the Labrador Current and delayed melting so sea ice and icebergs were found further south than usual this year.

In April 1912, the Titanic iceberg was only 1-200 km away from the much warmer water of the North Atlantic Drift (the warm ocean current moving northeast from the Gulf of Mexico to NW Europe under the influence of prevailing winds warming

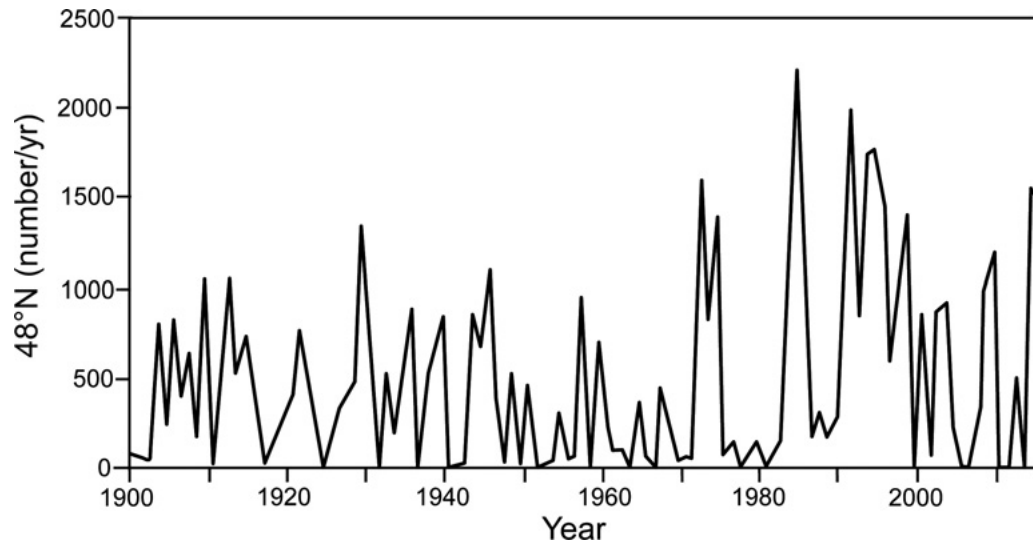


Figure 1.2: The total number of icebergs in the North-West Atlantic with a diameter of > 5 m crossed the latitude of 48° N for the year 1900 - 2014, with permission of Grant. R. Bigg

its climate), in which it would have quickly melted completely.

1.2 The origin of icebergs

The icebergs in the Labrador Sea originate from the Arctic and Greenland glaciers. Only a few Arctic icebergs survive in the Western North Atlantic for more than a few years and reach the Labrador Sea ([7, 37]). Most of the icebergs in the Labrador Sea calve from the glaciers on the western and eastern coasts of Greenland. Some icebergs from eastern Greenland (Figure: 1.1) go around western Greenland and Baffin Bay ([37]) and end in the Labrador Sea, and most of the icebergs that arrive in the Labrador Sea calve from the western part of Greenland. The mountain glaciers, ice caps, and ice sheets spawn icebergs. These are ice masses classified according to

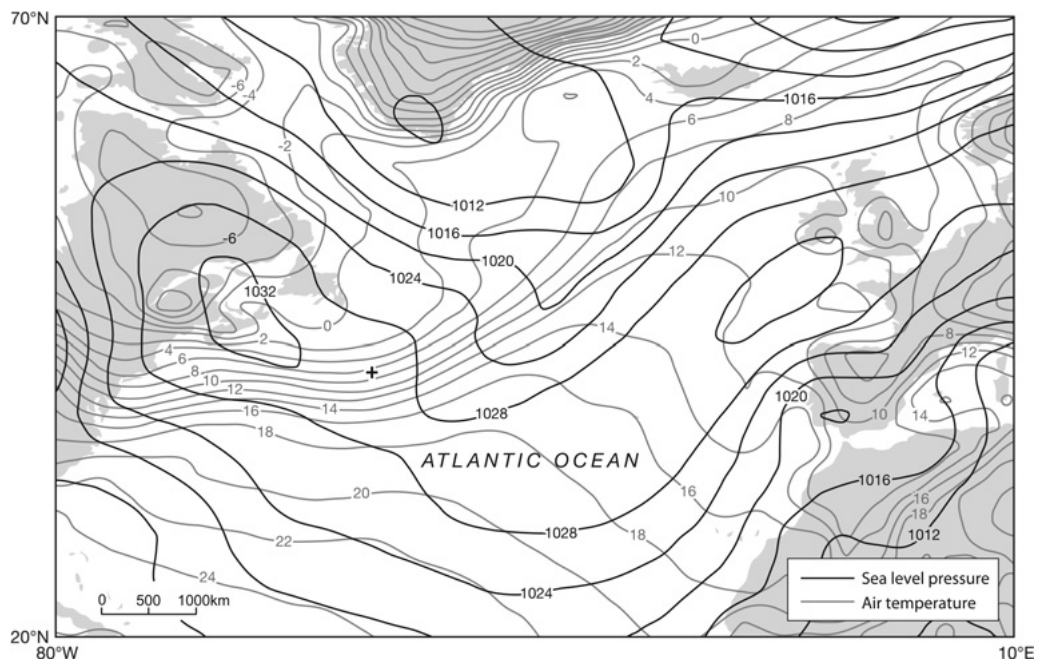


Figure 1.3: Chart for sea-level pressure and temperature on 15 April 1912 at 0000 GMT, with permission of Grant. R. Bigg and acknowledgement to G. P. Compo, J. S. Whitaker, P. D. Sardeshmukh([9])

the area covered.

Mountain glaciers (Figure 1.4) are relatively small, both in area and thickness, with a region of net accumulation in the upper and of net ablation in lower altitudes. A so-called equilibrium line separates these two regions. The altitude of the equilibrium line (ELA) is a function of annual variation in temperature and precipitation. The ELA will be lower where snow precipitation is higher in the winter, and it is relatively cold in the summer. In polar and subpolar glaciers that terminate in the sea, the ELA is higher and will usually be above sea level. For example, the Neumayer Glacier in South Georgia has an ELA of 550 m.

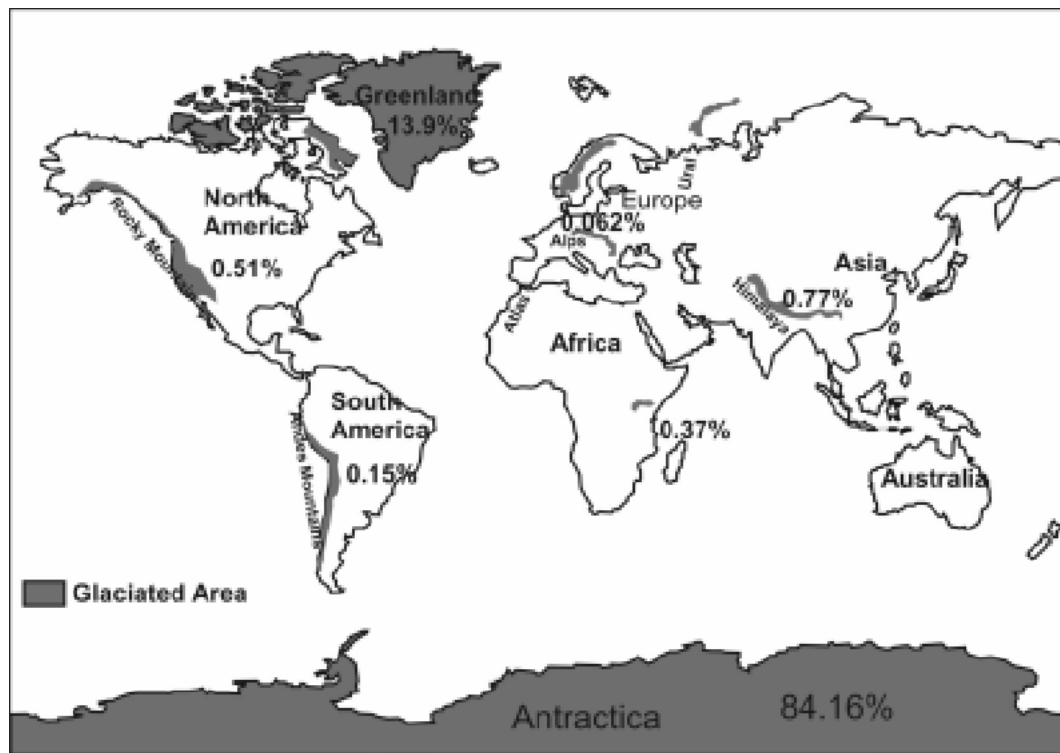


Figure 1.4: Distribution of glaciers in the World Ocean ([11])

1.2.1 Greenland Ice Sheet

Greenland is the second largest ice sheet on the planet, with glaciers covering 1.71×10^6 km² and volume of 2.85×10^6 km³ of ice. The freshwater released from the melting of the glaciers would be equivalent to 7.36 m of ocean sea level. North Atlantic storms strongly affect the ice sheet in the south end of Greenland (Figure 1.5).



Figure 1.5: Names of the main glaciers of Greenland, (https://www.nasa.gov/mission_pages/icebridge/multimedia/spr10/Greenland-3.html/)

One of the primary causes of the current rise in sea level is the melting of glaciers in polar areas. Since 1990, ice sheets have been monitored by satellites launched by the European Space Agency and NASA. They measure mass balance through altimetry,

o optical/radar imagery, and gravimetry. The Greenland Ice Sheet's mass balance is the net difference between ice gains from snowfall and ice losses from melting at its surface or under its floating ice tongues and the calving of icebergs from glaciers flowing into the ocean. On average, the Greenland Ice Sheet lost more ice through ablation than it gained through accumulation (Figure 1.6) in the years between 1992 and 2018 [34]. The total ice loss was 3.9 trillion tonnes, an average rate of 150 billion per year. The ice loss is accelerated by the increased melting of the surface during the summer [16]. Southwest Greenland loses ice because of higher melting due to the transport of warm air over the ice sheet.

1.2.2 Antarctic Ice Sheet

The Antarctic Ice Sheet is the largest ice sheet in the world, covering approximately 14×10^6 km² (more than eight times the area of Greenland). It has approximately 26.5×10^6 km³ of ice (more than nine times the Greenland Ice Sheet) and the freshwater equivalent of a 70 m sea level rise. It has two components: the West Antarctic Ice Sheet and the higher, more significant East Antarctic Ice Sheet. These two components are separated by the Transantarctic. Iceberg discharge accounts for Peninsula - Wordie, Prince Gustav, Larsen A, and B- decayed significantly due to global warming in recent decades, dumping massive icebergs into the ocean over a month or two.

The ice approaches the sea in three ways:

1. Fast-moving ice streams
2. Flow over the ocean surface as an ice shelf

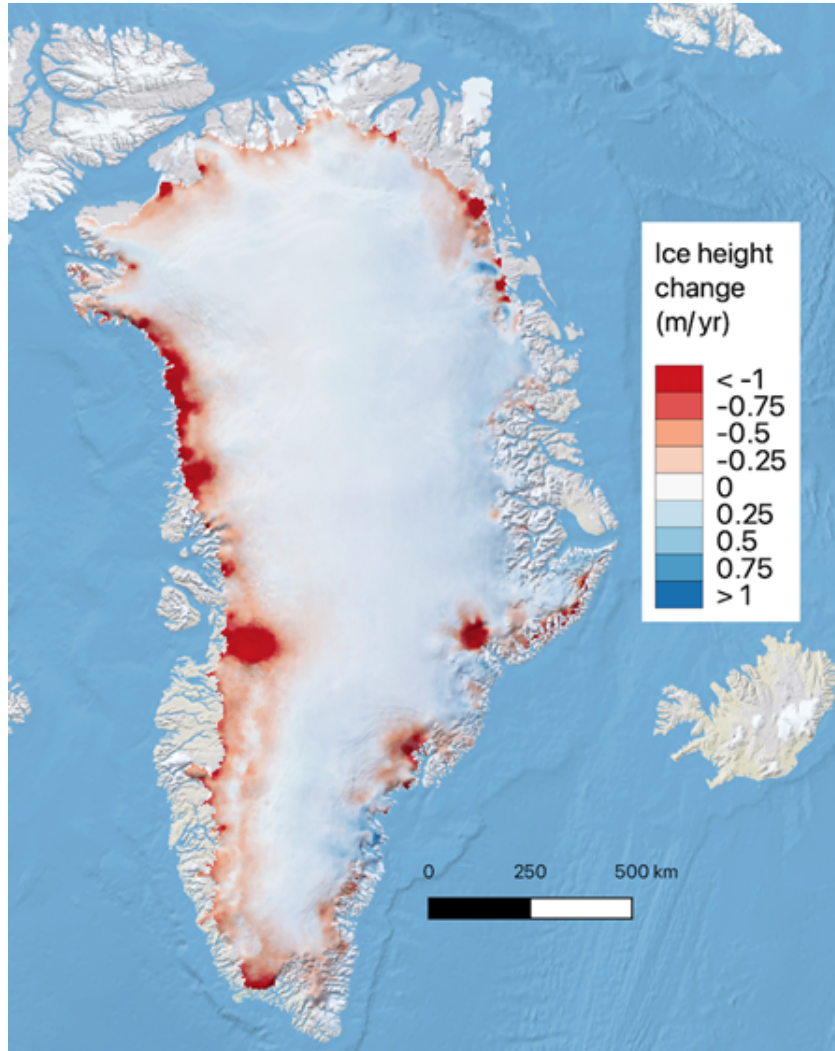


Figure 1.6: Rate of change of the mass of Greenland's glaciers with acknowledgement to Dr Tom Slater, (<https://www.antarcticglaciers.org/glaciers-and-climate/changing-greenland-ice-sheet/greenland-ice-sheet-mass-balance/>)

3. Slow flow directly into the ocean leading to grounded ice cliffs at the ice-ocean interface.

Ice streams are parts of the ice sheet where the ice flow rate is faster than the average flow rate for the ice sheet. They play an essential role in ice sheet stability and mass balance. Ice stream dynamics can be influenced by several factors, including geological, topographic, calving front, and hydrological factors. The most important of these is the effect of topography.

Ice shelves are the supply of ice that is less thick than seawater and, hence, they float. They have greater surface and basal melting and calving. Snowfall on the shelves' ice enables more ice to form. Ice was also added to the ice shelves' base due to the freezing of seawater circulation beneath the ice.

Ice cliffs form along the coast in area where the erosion of grounded ice front waves and melting keep speed with the ice supply.

1.3 Iceberg distribution

1.3.1 Methods of iceberg observation

Before 1913, data came from ship reports kept by the US Coast Guard [25]. Devoted ice patrols started in 1913 and remained the primary observation method until the 1950s, with formal patrols being suspended in 1917–18 and 1942–45 due to the World Wars. Aircraft had a more significant role in collecting iceberg data during and after World War II, first as a supplementary method and then as the main one.

A long-term Russian dataset of iceberg sightings in the Barents Sea dating back

to the 1930s is also available. Over time, this has also evolved from ship to aircraft surveys. The southernly extension of icebergs varies significantly, both yearly and over a longer duration, with considerable fluctuations of up to 8° of latitude; however, numbers on this are not published. Similar to the IIP dataset, this dataset predicts fewer icebergs in the warmer 1940s and 1950s but more icebergs in the final decades of the twentieth-century [21].

Since the 1980s, it has been possible to observe icebergs using satellite technology. Although icebergs were seen in visible images, the Southern Ocean's surface is frequently obscured by clouds, and it remains in the dark for several months of the year south of the Antarctic Circle. Therefore, more sensors with cloud-penetrating capabilities are required for efficient monitoring.

A scatterometer is a tool used to monitor icebergs longer than 5 kilometres. Large icebergs can be identified as high backscatter particles accompanied by a lower backscatter field of water or sea ice. This microwave radar equipment was initially designed to study ocean waves and their backscatter. Numerous scatterometers have been launched on various satellites dating back to 1978, but only since the launch of ERS-1 in 1992 [33] has there been continuous coverage. An outstanding record of giant icebergs' calving and trajectory is available, allowing us to highlight the numerous typical trajectories of smaller icebergs. The monitoring of small icebergs requires a high-resolution scatterometer. Synthetic Aperture Radar (SAR) is a type of radar used to create a two-dimensional or three-dimensional reconstruction of objects, and altimeters can detect icebergs that are tens of meters and $\sim 100 - 3000$ m, respectively. Altimeters measure the height of the sea surface by microwave backscatter and can resolve shorter distances than scatterometers. In essence, the iceberg acts as

a step in the signal. Assuming a generally tabular iceberg, the up and down steps of the signal indicate the size by measuring the height of the sea surface by microwave backscatter and can resolve shorter distances than scatterometers. Observations of icebergs sizes and numbers using this method can only go as far south as 70° S.

SAR is the iceberg detecting method with the highest accuracy and operates on the premise of giving a two-dimensional backscatter field rather than a one-dimensional footprint. It allows much higher resolutions than other existing methods. Although the larger swath on the Radarsat satellites has an effective resolution under 100 m, the conventional narrow beam of many types of SAR equipment can provide a resolution of just a few tens of metres. SAR equipment is typically utilized for high-resolution investigations of terrestrial features and is frequently turned off over the ocean making the analysis of icebergs by SAR somewhat limited. Except for coastal studies like Silva's [32], which used Radarsat1 to construct a seasonal image of the iceberg field surrounding Antarctica for September–October, 1997, unique acquisition requests are often required for specific times and locations for this sort of device.

As a result, SAR studies can not offer a reliable indicator of temporal variability. However, altimeter and scatterometer readings can, and they also offer year-round coverage. Due to the episodic nature of icebergs calving, the number of large icebergs varies throughout time (Figure 1.9). But the unpredictability of smaller icebergs reflects a mix of seasonal variability from the impact of sea ice and inter-annual variability in the regional flow. In austral summer, the seasonal signal in the Southern Ocean reaches a considerable high, as predicted given the peak calving season and the sea ice minimum.

1.3.2 Northern Hemisphere

In the North Atlantic, icebergs are generally found as far south as 40° N and as far east as 40° W and in the central North Atlantic (Figure 1.7). Although more uncommon, icebergs have been discovered over the past century along the east Siberian coast. Observations indicate that most of the central Arctic is iceberg-free. In the Barents Sea, icebergs are observed in the northern half and rarely approach North Cape in the south. Even though there are numerous locations in the Inside Passage, off the west coast, and in the Gulf of Alaska where glaciers calve into the sea, their icebergs are typically small and seldom extend past the fjord of origin or at most within the chain of islands along the coast.

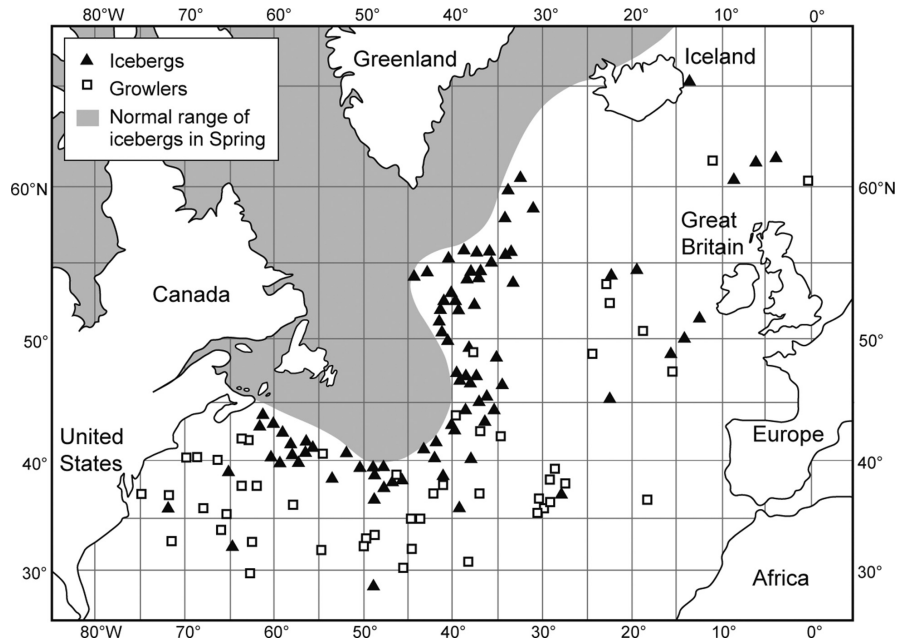


Figure 1.7: The North Atlantic mean iceberg zone, with permission of Grant. R. Bigg and acknowledgement to the International Ice Patrol

Icebergs' seasonal variability in the North Atlantic, Arctic, and nearby oceans can vary greatly depending on the region. There is a unique spring and early summer maximum (Figure 1.8) in the primary outlet region off Newfoundland, which is governed by a confluence of summer peaks in Greenland calving with delayed sea-ice in the Labrador Sea and all along the Labrador and Newfoundland coast. This also tends to happen in late winter, again likely indicating a discharge of icebergs as the sea ice begins its yearly retreat. The southernmost extent of the Barents water also seems significantly closer to the origin of the sea's icebergs [21]. Modelling indicates that, as anticipated, given the seasonal variation in calving, the most significant rate of iceberg egress through the Davis Strait into the northern Labrador Sea is in late summer and fall [37].

1.3.3 Southern Hemisphere

In the Southern Ocean, iceberg observation began in the second half of the eighteenth century. The International Geophysical Year of 1957 – 1958 necessitated frequent ship voyages across the Southern Ocean, and since then iceberg sightings have been systemically gathered. The iceberg observations in this region are gathered using a combination of visual and radar observations, and they typically contain details about icebergs' sizes and shapes. The most active research vessels in data collection and analysis publication have been Australian and Russian. The Australian data go back to the late 1970s and cover the Indian Ocean region, while the Russian data go back to 1957 and cover the entire Southern Ocean. These exhibit the presence of icebergs along the whole Antarctic coast, with concentrations in the Weddell Sea, the western

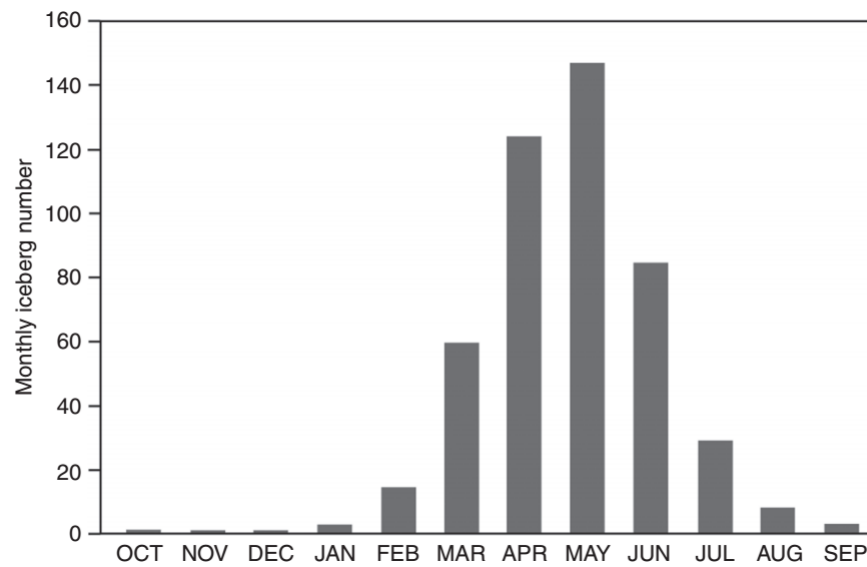


Figure 1.8: The figure represents the mean seasonal variation in iceberg number from the year 1900 to 2012, at 48° N, and this line extends from Newfoundland to 40° W, with permission of Grant. R. Bigg and acknowledgement to the International Ice Patrol

Indian Ocean [20], [29], and the two Pacific sides of the Ross Ice Shelf.

Icebergs are usually carried westward by the Antarctic Coastal Current from their initial locations along the Antarctic coast. In some areas, iceberg paths are connected to basin-scale gyres by local currents such as those in the western Weddell Sea or topographic steering near the Kerguelen (80-100° E) Macquarie (140-60° E) Ridges, which are responsible for carrying icebergs offshore into the central Southern Ocean. However, icebergs mostly stay south of 60° S, except for the Atlantic region, where the Weddell Gyre joins an Antarctic Circumpolar Current diversion that occasionally carries icebergs even north of 40° S [14].

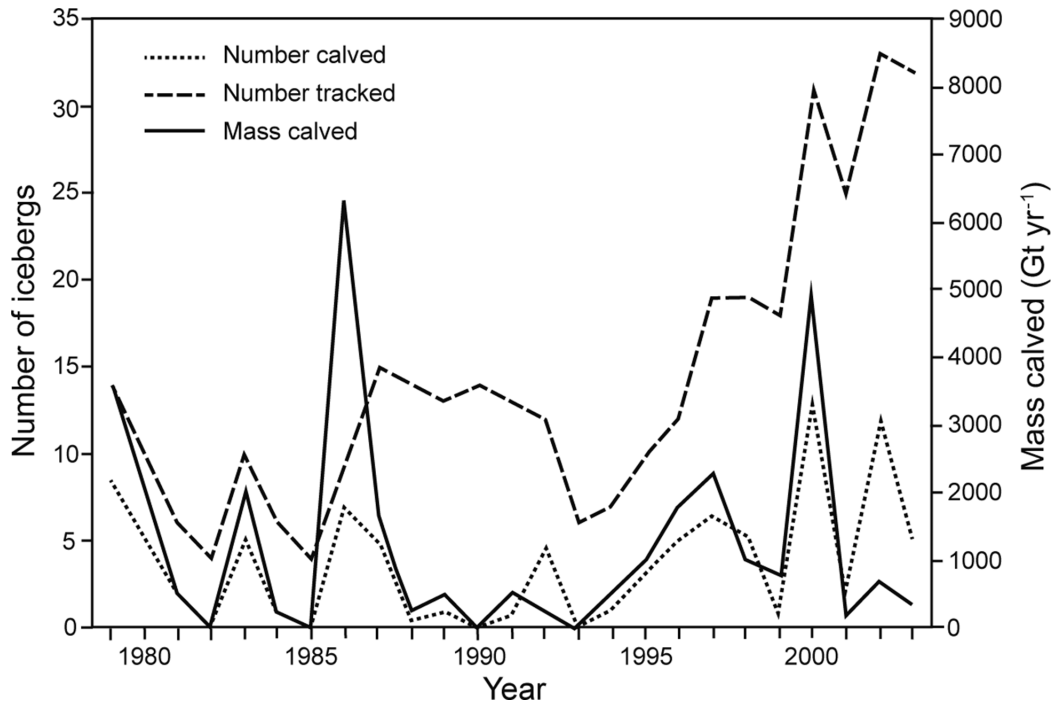


Figure 1.9: The number and mass of icebergs with a size > 18 km. The data is from the year 1979 to 2003, with permission of Grant. R. Bigg and acknowledgement to John Wiley and Sons.

1.4 Icebergs' impacts

1.4.1 Safety of the maritime and offshore industry

Icebergs are shipping hazards, and the RMS Titanic is one of the best examples of an iceberg accident. The IIP was established to monitor icebergs. Even though they are closely tracked, icebergs are still a threat to ships. In the last two decades, the number of icebergs in the NW Atlantic has increased. The following are some examples of recent ship hazards. On November 23rd 2007, the MV Explorer sunk in the northern Weddell Sea after having struck an iceberg in the Bransfield Strait. In the same area, a cruise ship called the MS Fram collided with an iceberg on December 28th 2007. The Russian fishing vessel Sparta was damaged by a submerged iceberg spur in December 2011 off the Antarctic coast east of the Ross Sea.

Icebergs are also a threat to fixed installations at sea, on the coast or under the sea floor. Giant icebergs can exert force of about 10^7 N. Fixed ocean platforms, such as drilling rigs or offshore wind generators, are highly prone to iceberg collisions. When the first undersea telegraph cable was laid across the North Atlantic from Ireland to Newfoundland in 1858, there was a risk of an iceberg scouring the sea floor and severing a costly communications link. Communications cables, oil and gas pipelines and even submarine tunnels can be damaged by icebergs. In the 1960s, communication wires offshore of Labrador were recorded as rupturing owing to iceberg scour.

Submarine facilities are protected against iceberg scouring in three main ways. The hazard can be identified early on, and the iceberg causing the problem may be removed. Also, sea-floor barriers like berms or concrete coatings can be used to

protect the facilities from icebergs [36]. However, the most cost-effective option is to bury the cable deep enough so that an iceberg's keel cannot harm it.

To avoid iceberg-related risks, it is necessary to detect and monitor icebergs. For the detection and monitoring of icebergs, radar and various satellite remote sensing instruments are used. Radar is employed as an IIP tool for ship and airborne systems. The former is commonly used in Arctic seas for research and danger avoidance. In 1990, the first ground-based detection system was installed at Cape Race on Newfoundland's farthest south-eastern coast. Sea clutter disrupts the detection of icebergs. Remote sensing is another approach used in the detection of icebergs. Huge icebergs may be spotted using devices with coarser pixel resolution, but smaller icebergs require a higher resolution instrument. Landsat provides remote sensing data from the world's most prolonged and continuous collection of space-based data with moderate resolution and Moderate Resolution Imaging Spectroradiometer or MODIS is a sensor used for earth and climate measurements. This sensor operates on the Terra and Aqua satellites, which are used in the early detection of icebergs. Icebergs with a length greater than 5 km are monitored with a microwave scatterometer. SAR is the most common device used for regular iceberg monitoring as well as for research.

The prediction of iceberg risk is a key element in avoiding accidents. Prediction can take two forms: a broad climatological viewpoint on iceberg danger for an area or a direct forecast of the movements of an individual iceberg. The first is crucial for assisting shipping and maritime services by providing general awareness of where they may encounter icebergs and the likelihood of such an encounter. Modelling single iceberg trajectories can provide a more thorough perspective of the risk posed by individual icebergs.

As a result, a combination of national and commercial services and a worldwide consortium of ice hazard services, Polar View, serves as a conduit for connecting maritime operators with various ice service providers. In this case, the Canadian corporation C-CORE is the specific provider of worldwide iceberg monitoring. ICE-MAR is a European corporation launched in late 2013 that aims to offer information for the European Arctic. These services provide information regarding ice risks; this information is often on ice in general but is also on the presence of icebergs in many circumstances.

When an iceberg danger has been recognized and no action to avoid the iceberg is practicable, methods to eliminate the hazard are necessary. One technique is to detach marine platforms from the sea floor and move them away from the hazard. Several naval oil rigs now have this capacity by using moorings rather than permanent platforms, with differing degrees of ease with which the platforms are withdrawn. It is more common for the iceberg to be towed or pushed onto another route a minor deviation is required to remove the risk. Towing is expected in oil fields off the coast of eastern Canada, which is where the practice was invented. Tugging is usually done by encircling the iceberg with a floating line, sending out steel cable from the anchor handling tug supply vessel to stabilize the rope, and then towing the iceberg to safety. Icebergs can also be removed for various purposes, such as for supplying freshwater or to be transformed or destroyed to eliminate or deflect the hazard.

1.4.2 Icebergs as a freshwater source

After Cook pioneered the utilization of icebergs as a source of fresh water(Figure 1.10), it became a watering technique employed on occasion by sailing ships in the frigid and island-less Southern Ocean. Icebergs are also a source of ice, which is used as a coolant, and the subsequent recorded use of icebergs for water began in the second quarter of the 19th century when icebergs were towed from a freshwater calving source in the Chilean Andes to Valparaiso in southern Chile to provide refrigeration in local breweries.

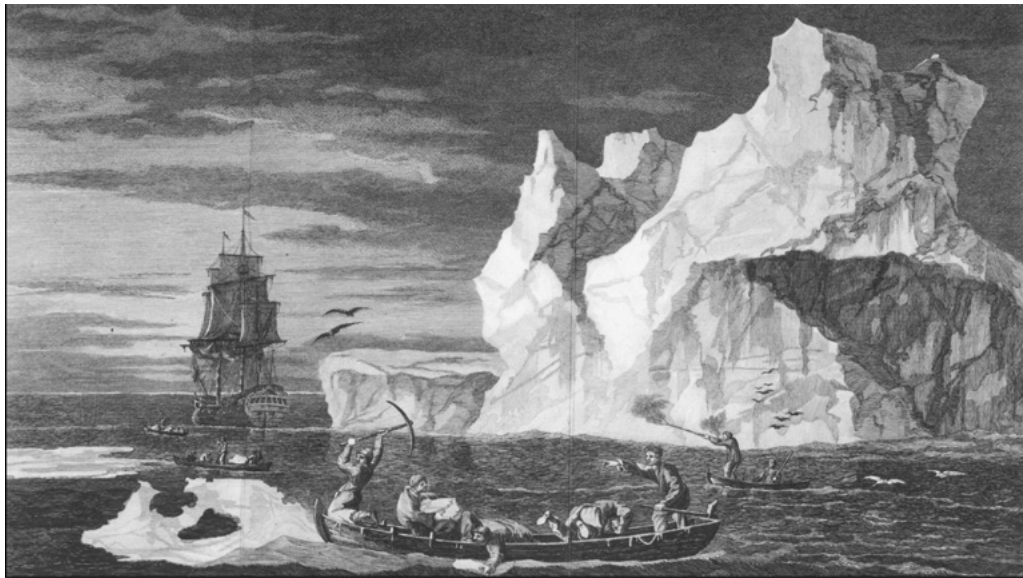


Figure 1.10: Captain Cook obtaining fresh water from an iceberg, with permission of Grant. R. Bigg and acknowledgement to Captain Cook

Weeks and Campbell reintroduced the notion of dragging icebergs to dry locations and then using their water for agricultural and personal use in a series of studies published

in 1973. Their main contribution was to show for the first time that the concept was theoretically feasible in terms of towing, iceberg preservation, and economic cost. Weeks and Campbell's vision in 1973 was that Antarctica was a significant source of icebergs, and there were practical routes for moving large tabular icebergs from the Ross Sea to the west coast of South America, as well as from the Amery Ice Shelf of the Indian Ocean sector of the Southern Ocean to southern Australia. They noted several constraints, including melting during the journey, towed iceberg stability, engineering and power needs for specially built towing vessels, and the environmental implications of melting icebergs both on the way and at the destination.

At the time, Saudi Arabia recognized the possibility of altering its arid environment by importing Antarctic freshwater as ice. A large international conference sponsored by the Saudi government was held in Ames, Iowa brought together academics from across the non-Soviet bloc. Campbell and Weeks recognized that they needed to fix several problems to continue this project. The first problem faced by the dormant industry was locating adequate icebergs. Because of extensive IIP monitoring, this issue would be mitigated in eastern Canada. However, the icebergs here are less likely to be appropriate for long-distance towing because of their smaller size or odd shape.

Because the primary goal of towing icebergs is to deliver fresh water to the destination, minimizing melt along the way is a top concern. Exposure to warmer waters as the glacier drifts equator-ward combined with the significant erosion and fracture caused by Southern Ocean storms will melt the iceberg before it reaches land. As a result, icebergs never reach the southern continents or islands north of 40° S on their own.

As a result, some form of insulation from both temperature and waves is desirable. A plastic or foam jacket was envisioned in the 1970s, but different designs have arisen in patents since then. Nonetheless, this is a significant practical issue. When a towed iceberg arrives at its location, the following engineering challenge is determining how to melt and catch the freshwater. The difficulty is transferring heat to the iceberg while keeping the meltwater from mixing with the surrounding ocean. Atmospheric heating is a slow process, so heat for melting might be supplied by waste energy from adjacent heating facilities or by using floating solar power plants. Another option is to use explosives to shatter the iceberg into smaller bits that will melt faster. To avoid contamination, liquid oxygen explosives should be used for this purpose.

1.5 Physics of icebergs

Iceberg models simulate the paths and evolution of icebergs. They are initiated based on information about (a) appropriate calving sites, (b) approximate calving rates, and (c) a spectrum of typical sizes appropriate to a given calving rate [7]. The model equations describing icebergs' paths are based on knowledge about iceberg dynamics.

1.5.1 Basic forces driving iceberg motion

The equation of motion [7] is given by

$$M \frac{d\vec{v}_i}{dt} = -Mfk \times \vec{v}_i + F_w + F_a + F_s + F_r + F_p. \quad (1.1)$$

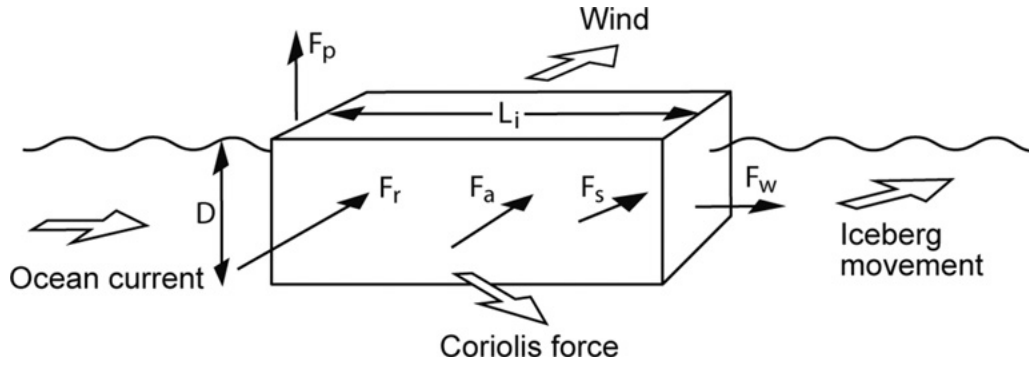


Figure 1.11: Schematic representation of the forces responsible for the movement of icebergs

Where M - Mass of the iceberg

\vec{v}_i - Horizontal velocity.

f - Coriolis parameter.

t - time.

F_p - Horizontal pressure gradient force exerted by the water on the iceberg volume the iceberg.

F_w - Drag exerted by the submarine part of the iceberg by the surrounding water.

Generally, the drag force is,

$$F_j = \frac{1}{2} \rho_j C_j A_j |\vec{v}_j - \vec{v}_i| (\vec{v}_j - \vec{v}_i). \quad (1.2)$$

where j - refers to water (w), air (a), or sea-ice (s) Wave radiation force is significant for loose packed ice or open water.

where L is the length of the iceberg normal to the incident wave.

The pressure gradient force is the impact of the slope of the sea surface,

$$F_p = -M \frac{\Delta P}{\rho_w}. \quad (1.3)$$

where P is the pressure field.

The horizontal pressure gradient, $\nabla_h p$, is due to the variation of the sea surface height in the horizontal; it is the same pressure gradient that drives the ocean current.

The force on the iceberg is

$$\vec{F}_p = -\frac{M}{\rho_w} \nabla_h p = Mg \nabla_h \eta = Mf \vec{n} \times \vec{v}_g. \quad (1.4)$$

where ρ_w is the seawater density, η is the sea surface height (SSH) and \vec{v}_g is the geostrophic velocity of the ocean current. Equation (1.4) shows that either SSH measured by a satellite altimeter or the geostrophic velocity can be used to compute \vec{F}_p . By moving the Coriolis term in the brackets to the right-hand-side of (1.1) and combining it with \vec{F}_p we obtain

$$\vec{F}_{Cp} = Mf \vec{n} \times (\vec{v}_g - \vec{v}_i). \quad (1.5)$$

Henceforth, we call this term the combined Coriolis and pressure gradient force.

The dominant forces responsible for the iceberg movement are the water drag (F_w) and the pressure gradient force (F_p). These two forces contribute approximately $70 \pm 15\%$ [7]. The Coriolis and the air drag forces contribute $\sim 15\%$ [7] each. In most conditions, the sea-ice drag force is negligible, except when the sea-ice is compact and thick and the iceberg flows with the sea-ice pack. The contribution of wave radiation force is $\sim 5\%$ [7]. In the Arctic, the Coriolis and the air drag forces are more important than the water drag force when the currents tend to weaken.

1.5.2 Iceberg thermodynamics

Thermodynamic processes may cause changes in an iceberg's configuration. This involves numerous mechanisms to melt the ice, above or below water. It is feasible to expand the iceberg's size below the waterline in sufficiently cold water by freeze-on or above-water thickness via snowfall. The most crucial process in modifying the size and shape of an iceberg is melting. Melting can occur due to turbulent heat transfer at the iceberg's base, buoyant convection-induced melting on the submarine sides, wave erosion at the air-sea interface on the iceberg's sides, sublimation from aerial surfaces, and the absorption of solar radiation and sensible heat from the atmosphere.

A significant loss term is 'basal' melting, which happens due to the transfer of heat from the surrounding water, which generally has a higher temperature than the ice. The relative velocity of the iceberg through the water produces turbulence in the boundary layer around it, which enhances melting. The latter is defined by the linearised equation of state [31], which is

$$T_B = aS_B + b + cp_B. \quad (1.6)$$

T_B - Temperature in the water at the base of the iceberg.

S_B - Salinity in the water at the base of the iceberg.

$$a = -5.73 \times 10^{-2} \text{ } ^\circ\text{Cpsu}^{-1}$$

$$b = 8.32 \times 10^{-2} \text{ } ^\circ\text{C}$$

$$c = -7.61 \times 10^{-4} \text{ } ^\circ\text{Cdbar}^{-1}$$

p_B - Water pressure at the base.

The equation of conservation of heat is defined by.

$$|u|\gamma_T(T_\infty - T_B) = -M_T \frac{L_H + \Delta T c_i}{C_w}. \quad (1.7)$$

The conservation of salt,

$$|u|\gamma_S(S_\infty - S_B) = -M_T S_B. \quad (1.8)$$

where $|u|$ is the water speed relative to the iceberg base,

γ_T ($= 6 \times 10^{-4}$) - coefficients of heat transfer from water to ice, respectively.

γ_S ($= 2.2 \times 10^{-5}$) coefficients of salt transfer from water to ice

T_∞ - far-field temperature

S_∞ - far-field salinity

L_H - Latent heat of fusion of ice

c_w ($\sim 4000 Jkg^{-1}K^{-1}$) - specific heat capacities of water

c_i ($\sim 2010 Jkg^{-1}K^{-1}$) - specific heat capacities of ice.

ΔT - The temperature difference between the iceberg core and the bottom surface.

M_T - Turbulent melt rate. Using 1.6, S_B and T_B can be eliminated from 1.7 and 1.8, the quadratic equation for M_T .

$$a_1 M_T^2 + a_2 M_T + a_3 = 0. \quad (1.9)$$

$$a_1 = \frac{L_H + \Delta T c_i}{|u| c_w \gamma_T}. \quad (1.10)$$

$$a_2 = T_\infty - b - cp_B - u\gamma a_1. \quad (1.11)$$

$$a_3 = -|u|\gamma_S(T_\infty - (aS_\infty + b + cp_B)). \quad (1.12)$$

The term $(T_\infty - (aS_\infty + b + cp_B))$ represents the difference between the water temperature in the far-field and its freezing point at the same pressure at the base of the iceberg. When this term is positive, M_T will be negative, which implies iceberg melting. Comparable heat transmission happens along the submerged sides of an iceberg due to buoyant convection. The following empirical equation defines the melting rate.

$$M_v = 7.62 \times 10^{-3}T_w + 1.29 \times 10^{-3}T_w^3. \quad (1.13)$$

T_w denotes the water temperature at the iceberg's sides in degrees Celsius. T_w will be comparable to T_B throughout the winter half of the year. However, when a shallower mixed layer occurs during the summer, T_B is likely to be different and usually colder than T_W along much of an iceberg's sides.

Wave erosion is one of the most significant melting terms. It depends on the sea surface temperature(T_s) and the presence of sea ice. The more sea ice there is, the more surface waves are damped, decreasing the sea state for a given wind speed. The melting rate,

$$M_e = \frac{1}{12}(T_s + 2)(1 + \cos(I_c^3\pi))S_s. \quad (1.14)$$

I_c - sea-ice concentration

S_s - sea state

The other factors above-water, air-sea interface on the iceberg's sides, sublimation from aerial surfaces, absorption of solar radiation and sensible heat from the atmosphere have negligible effects.

1.6 Iceberg modelling

The iceberg models are essential tools for studies of not only present days iceberg trajectories and comprehending the iceberg dynamics but also for exploring the geologically recent and present-day circulation of the relatively difficult-to-access polar oceans. Because of the large number of icebergs originating from the major glaciers, the numerical models usually use simple parameterizations of iceberg shape, a and water drag forces, and melting. The shape of the icebergs is normally assumed to be a cuboid with drag forces parameterized in terms of drag coefficients. The melting process is separated into several components - basal melting, sub-surface melting due to buoyant convection, wave erosion and surface melting due to the latent, sensible and solar heat fluxes [6].

The iceberg velocity is found from the momentum equation which is Newton's second law. It is a nonlinear equation and it's solution is found by using a numerical method for solving ordinary differential equations. The forces acting on the iceberg are computed using observational or reanalysis ocean and atmospheric data and include the Coriolis force, water drag force, air drag force, wave radiation force, and sea-ice drag force. The iceberg trajectories are then computed until they either hit the ground or lose all of their mass below 0.25% of the smallest size class. When bergs enter shallow waters with depth equal to or smaller than for their draught, they are

stranded and permitted to melt until they are small enough to proceed.

The previous model studies demonstrated that the majority of bergs calving from Western Greenland move west and south displaying an anticlockwise rotation. The majority of bergs do actually avoid Baffin Bay and traverse the very southern end of Davis Strait. The distribution of icebergs in the Labrador Sea depends significantly on the seasonality and size distribution of bergs calving from Greenland [6]. The iceberg distribution in the Western North Atlantic depend on the glacier calving rates and, consequently it can be used to assess the mass balance of the Greenland Ice Sheets.

[23] included interactive icebergs into a full three-dimensional CGCM created for climate projections in the twenty-first century. The coupled system used information about the frozen freshwater discharge from land to determine the rate of calving. These author modelled icebergs as point particles whose trajectories and volume evolved in accordance with equations of momentum and mass balance. They simulated roughly 100,000 individual particles combined in clusters and used the model results to estimate the geographical distribution of the meltwater.

Some models assume that there is a balance between the forces acting on the icebergs and therefore the derivative of the velocity or iceberg acceleration is negligibly small. This allows obtaining an analytical expression for the iceberg drift. [35] used an analytical model to study the key physical mechanisms that govern iceberg motion. High-resolution surface velocity and temperature data of the ocean state were used in this study to estimate are used to forces acting on icebergs and their motion.

1.7 Motivation of the study

Climate change has important impacts on the cryosphere of the planet. A significant decrease has been observed in Arctic ice water and land ice and snow. One of the areas mostly powerfully affected by climate warming is Greenland.

The recent climatology of Greenland allows us to understand the disequilibrium of ice configuration. The interannual variability of the Greenland Ice Sheet mass budget is controlled by surface ablation through meltwater run-off throughout 2000-2012. High surface ablation and meltwater run-off happened in 2012 (a high melt year) due to the excess atmospheric heat in Greenland. Nowadays, western Greenland has four times the regional imbalance of eastern Greenland. This imbalance is due to the strong east-west gradient in snowfall accumulation. Northwest Greenland caused 79 ∓ 12 *mm* equivalent to sea level rise throughout 2000-2019. In northeast Greenland, the modest equivalent sea level is 24 ∓ 30 *mm*, but it rises to 65 ∓ 8 *mm* in the 2012 climate [8]

The decay of Greenland's glaciers increases the freshwater input to the ocean, partly due to river discharge and partly due to the calving of icebergs. Most icebergs do not melt locally at the area of their calving root, and they drift in the ocean at a considerable distance. They are an efficient source of freshwater in the area of their melting, which can be hundreds of thousands of kilometres away from Greenland. Understanding the processes of iceberg drift and melting is essential for understanding the remote impact and processes of glacier decay on the surface ocean freshwater budget. The focus of this study is the development of iceberg models with improved prediction of iceberg paths and melting.

Chapter 2

Model, Data and Methodology

The paper "Effects of Wind, Waves, and Currents on Icebergs and Surface Floats in the Labrador Sea: A Modeling Study" [26] is published.

Contributions to the paper: original draft preparation, methodology, , data acquisition, and model simulation and visualization.

2.1 Data sets

In this thesis we present results from a case study of year 2008. The forcing data (Figure 2.2) include ocean currents, wind velocity and characteristics of surface waves. The latter consist of the mean wave period, T , mean wave direction, θ , and significant height of combined wave and swell, H_s . The wind and surface wave characteristics are derived from the hourly ECMWF reanalysis (ERA5) [17] with a spatial resolution of 0.25 degrees. The ocean current, sea-surface height and sea surface temperature are from the MERCATOR Ocean International daily reanalysis provided by Copernicus Programme (<https://marine.copernicus.eu/>). All forcing data are spatially interpo-

lated on $0.05^0 \times 0.05^0$ numerical grid for the region $45^0N - 70^0N$, $70^0W - 40^0W$ (Figure 2.1.)

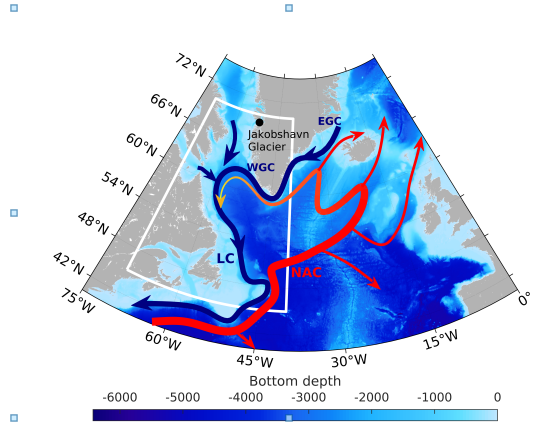


Figure 2.1: Map of the computational domain and circulation in the subpolar North Atlantic. The arrows show major currents in the subpolar gyre, including the North Atlantic Current (NAC), the Eastern Greenland Current (EGC), the Western Greenland Current (WGC), and the Labrador Current (LC).

2.2 Model and Methodology

A common assumption that the icebergs are of a cuboid shape of length L , width W and height (H) is used. A typical ratio of the iceberg horizontal dimensions is $L/W \approx 1.5$ [?]. In the vertical, the ratio of the subsurface depth or the draught of an iceberg to the total height can be easily found as

$$\frac{H_w}{H} = \frac{\rho_i}{\rho_w}, \quad (2.1)$$

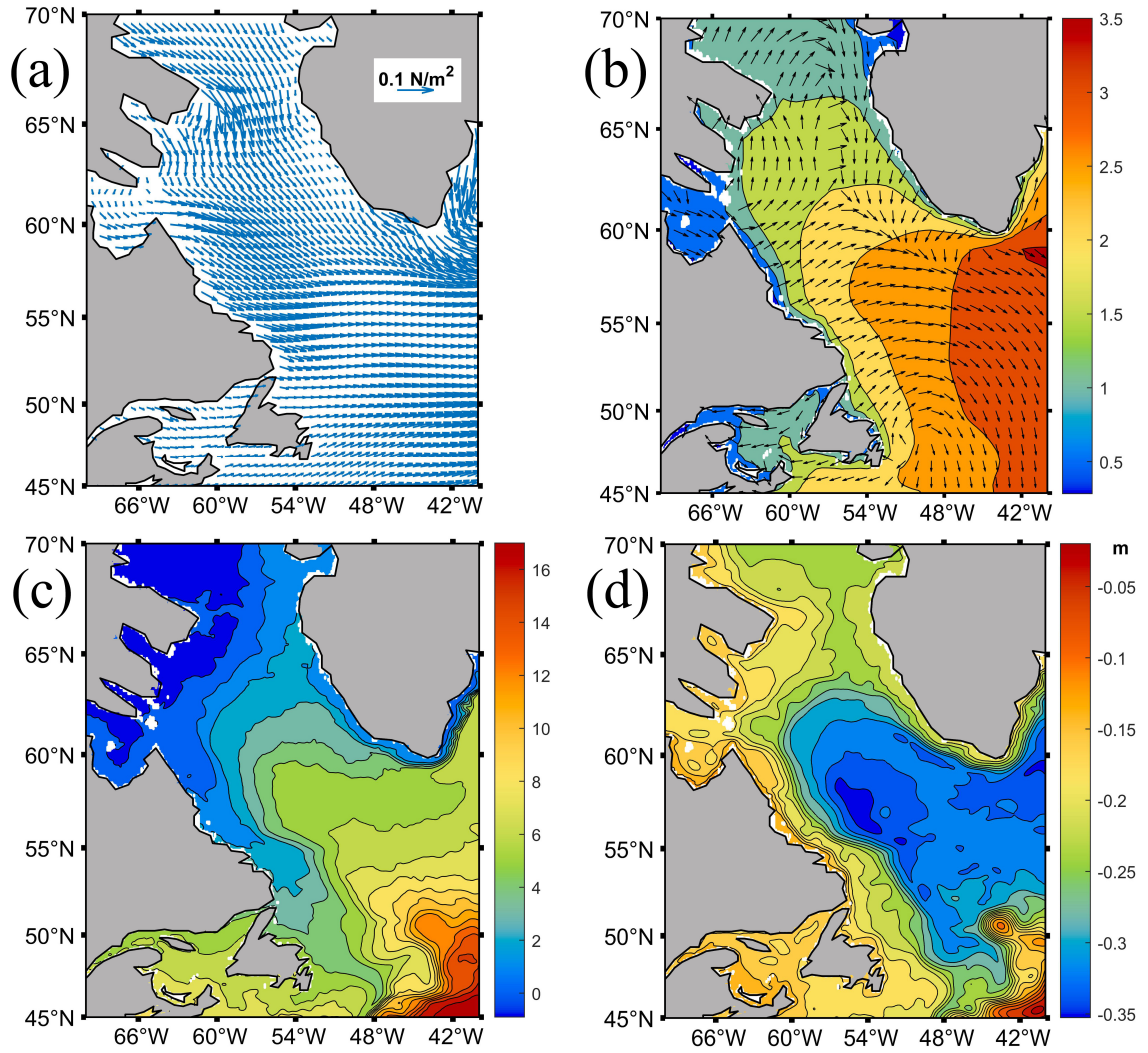


Figure 2.2: Annual mean surface forcing used in the iceberg model (a) surface wind stress; (b) direction and mean height of surface waves; (c) sea surface temperature (contour interval 1° C), (d) sea surface height (contour interval 2 cm).

where $\rho_i = 900 \text{ kg/m}^3$ is the density of sea-ice and $\rho_w = 1022 \text{ kg/m}^3$ is the seawater density. The above-water height ("freeboard" in nautical terminology) is then $H_a = H - H_w$. Observations show that icebergs can be divided into several categories according to their size [15]. Here, we choose 8 categories of icebergs (Table 2.1) which correspond to categories 2-5 and 7-10 in [15].

Table 2.1: The iceberg categories.

Category	Length, m	Height, m	Mass, kg
2	100	67	4.1×10^8
3	200	133	3.3×10^9
4	350	175	1.3×10^{10}
5	500	250	3.8×10^{10}
7	900	250	1.2×10^{11}
8	1200	250	2.2×10^{11}
9	1600	250	3.9×10^{11}
10	2200	250	7.4×10^{11}

To complete the iceberg drift model we need to obtain the current velocity $\vec{v}(z)$ in the surface layer of the ocean. It is defined as a sum of the geostrophic and ageostrophic components, $\vec{v} = \vec{v}_g + \vec{v}_{ag}$, where \vec{v}_{ag} is, in turn, can be decomposed into a number of components such that

$$\vec{v}_{ag} = \vec{v}_t + \vec{v}_{nl} + \vec{v}_E + \vec{v}_S. \quad (2.2)$$

The first two terms in the RHS of (2.2) occur due to time tendency and non-linearity of the momentum equations of water. By considering the equation 1.1, in the surface

layer, $p = g\rho_o\eta$

η = sea surface height

The geostrophic approximation

$$-fv_g = \frac{1}{\rho_o} \frac{\partial p}{\partial x} = -g \frac{\partial \eta}{\partial x} \quad (2.3)$$

When substituting the 2.3 to 1.1, we can get the equation for time tendency and non-linearity of the momentum equations of water and can be written as [10, 1]

$$\vec{v}_t = -\frac{g}{f^2} \vec{\nabla} \eta_t, \quad (2.4)$$

$$\vec{v}_{nl} = -\frac{g^2}{f^3} J(\eta, \vec{\nabla} \eta), \quad (2.5)$$

where J is the Jacobian operator (the determinant of the matrix of partial derivatives), which in Cartesian geometry is $J(A, B) = A_x B_y - B_x A_y$. The temporal derivative or tendency, η_t , is calculated via finite difference between two successive data fields in a sequence. Note, that the ageostrophic components \vec{v}_t and \vec{v}_{nl} are routinely computed in laboratory experiments with high-resolution altimetry [3, 4, 39, 24, 40, 2].

The remaining two terms in (2.2) are the Ekman and Stokes components respectively [38, 19]. They account for the Ekman currents due to wind stress at the surface of the ocean as well as the Stokes drift due to surface gravity waves. Classic Ekman surface-boundary-layer theory describes a wind-stress induced current and its variation with depth such that

$$\vec{v}_E = \frac{d}{\rho_w A_z (1+i)} \vec{\tau} e^{(1+i)z/d}, \quad (2.6)$$

where $d = (2A_z/f)^{1/2}$ is the characteristic depth of the Ekman layer, $i = \sqrt{-1}$, A_z is the effective vertical viscosity in the upper ocean and $\vec{\tau}$ is the wind stress. Note, that A_z cannot be measured directly by remote means but it was shown [12, 30] to be related to the wind velocity U_{10} which can be obtained from the satellite data. A useful approximation is $A_z \simeq 1.2 \times 10^{-4} U_{10}^2$ where all quantities are in SI units. The last term \vec{v}_S accounts for the modification of the Ekman boundary layer by surface gravity waves and can be written as [22, 28, 38]

$$\vec{v}_S = \frac{\vec{V}_S(z=0)}{2(dk)^2 - i} (ie^{2kz} - kde^{(1+i)z/d}), \quad (2.7)$$

where \vec{V}_S is the Stokes drift given by [27]

$$\vec{V}_S = a^2 \sigma \vec{k} e^{2kz}. \quad (2.8)$$

where a is the wave amplitude, \vec{k} is the wavenumber vector and $\sigma = (gk)^{1/2}$ is the wave frequency related to the wavenumber k via a dispersion relation for deep water waves. The wave amplitude can be obtained from the significant wave height data, $a = H_s/2$. Historically, the heights of the ocean waves were observed in units of significant wave heights. Here the significant wave heights are obtained from the output of wave prediction models and used to compute the velocity of Stokes motion. The direction and magnitude of the wave vector \vec{k} can be obtained from the remotely-sensed data on the mean wave direction and period; k is related to the wave period T via the dispersion relation, such that $k = 4\pi^2/gT^2$.

Surface floats or icebergs are considered to be Lagrangian particles and their trajectories are computed by integration of the kinematic equation

$$\frac{d\vec{r}}{dt} = \vec{v}(\vec{r}, t), \quad (2.9)$$

where $\vec{r} = (x, y)$ is the position vector of a float or an iceberg. Floats are driven by the surface velocity, such that the RHS of (2.9) is simply the (Eulerian) velocity of the ocean current, \vec{v} . For icebergs, the RHS of (2.9) becomes the iceberg velocity, \vec{v}_i . Computation of float trajectories requires solving the single equation (2.9). In contrast, computation of iceberg trajectories involves solving several equations simultaneously including the momentum equation (1.1), equations (1.9, 1.13, 1.14) describing melting and erosion and the kinematic equation (2.9). Numerical integration of these equations employs the 4-th order Runge-Kutta method.

Icebergs of each category are seeded over an area of $1^\circ \times 1^\circ$ offshore of the Jakobshavn glacier which is a major source of icebergs in the western Greenland [18]. The initial condition for iceberg velocities is obtained as a solution of the stationary version of equation (1.1) with the forcing for 1:00 am on January 1st, 2008. The drag \vec{F}_w is calculated by averaging over the depth of the submerged part of the iceberg. Following [35], we assume that icebergs are oriented at a random angle relative to the wind and current. In this case, the long-term mean of the vertical surface areas under- and above-water is given by

$$A_w = 2/\pi(L + W)H_w \quad (2.10)$$

$$A_a = 2/\pi(L + W)H_a \quad (2.11)$$

2.2.1 Time stepping

The model equation of iceberg motion is a nonlinear second order Ordinary Differential Equation. The method of solution is based on the y -th order Runge-Kutta method.

Chapter 3

Results

In this Section we describe the results of modeling of the trajectories of surface floats and icebergs for the year 2008 as well as the analysis of the relative importance of different components of the environmental forcing.

3.1 Surface floats

The Global Drifter Program has deployed worldwide drifters since 1979. They can follow the surface currents with minimal slippage and collect information about the essential climate variables. Like the icebergs, the floats are Lagrangian in terms of the description of their positions and velocities. The broad availability of drifters' data makes them helpful information for understanding and predicting the Lagrangian motion at the ocean surface. At the same time, there are also essential differences between the dynamics of the floats and icebergs. Understanding the differences in the kinematics of the icebergs and drifters is critical for using and assimilating the drifters' data in improving iceberg model predictions.

Figure 3.1 shows the annual mean surface velocity and its components, namely, the quasigeostrophic, Ekman and Stokes velocities. Here, the term "quasigeostrophic" is used for the sum of the geostrophic, nonlinear and time-tendency components of the velocity. The standard deviation of velocity is computed as:

$$u_{std} = \sqrt{\frac{1}{N} \sum_{n=0}^N |\vec{u}(n) - \vec{u}_m|^2} \quad (3.1)$$

where $\vec{u}(n)$ is the velocity at time step n and \vec{u}_m is the vector of annual mean velocity. The quasigeostrophic velocity (Figure 3.1 b) has its highest magnitude in the East and West Greenland currents, and in the Labrador Current. These boundary currents are steered by the bottom topography and are intensified over the continental slope. They are strengthened by winds in the fall and winter seasons and decrease in the summer. The quasigeostrophic currents in the southern part of the region are influenced by the North Atlantic Current. This current is subject to high mesoscale eddy variability (Figure 3.1 b). The annual mean Ekman currents have predominantly southward to southwestward directions (Figure 3.1 c). The variations of the Ekman transport is most significant along the west coast of Greenland. The Stokes velocities have the smallest contribution to the annual mean surface currents (Figure 3.1 d). They have larger magnitudes in the southeastern part of the region.

A comparison of the mean surface current (Figure 3.1 a) with its individual components shows that it is quasigeostrophic to a certain degree in the boundary current along the coasts of Labrador and Greenland. In the northern part of the region and in the Baffin Strait the Ekman component has a significant contribution (Figure 3.1 c) to the mean and standard deviation of velocity. The time series show that the Ekman

and Stokes components can intensify locally in the areas of passing weather disturbances. These intensification can affect the surface velocity locally for a relatively short period of time of several days.

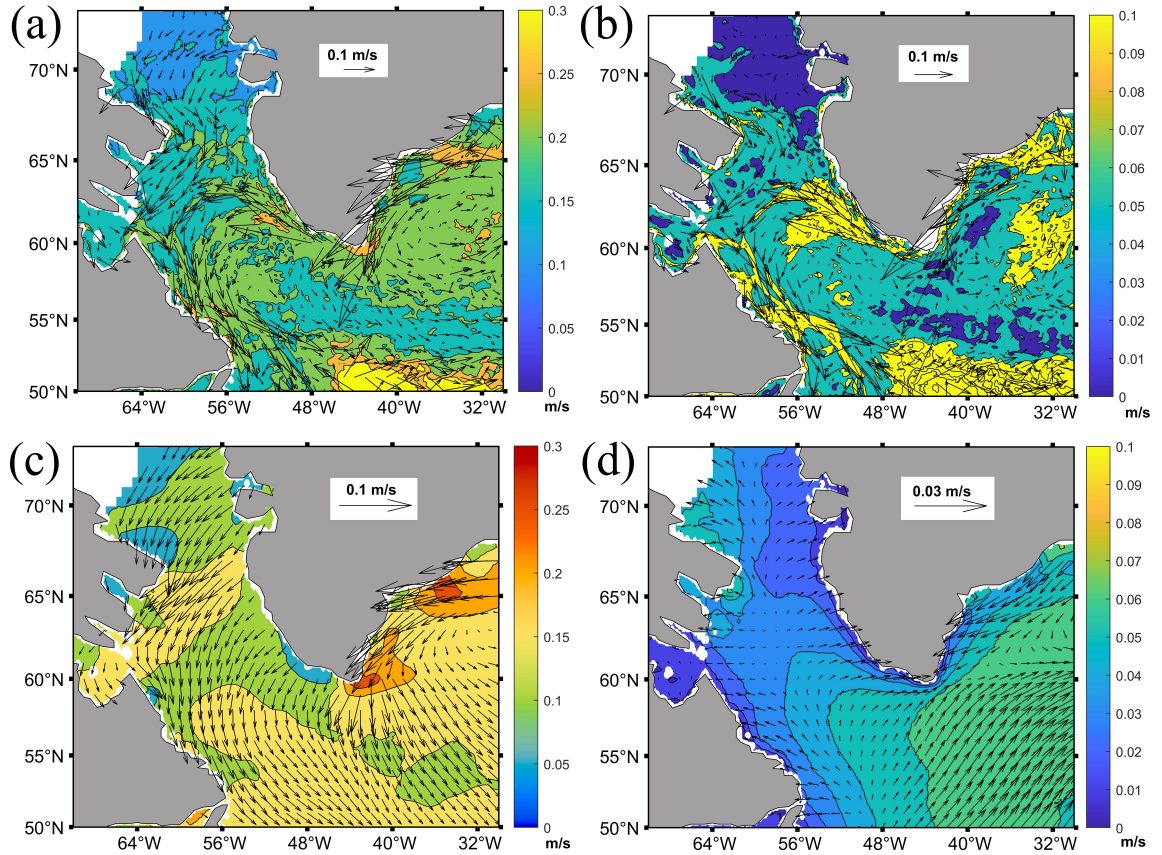


Figure 3.1: Annual mean and contours of standard deviation of (a) ocean surface velocity (contour interval 0.05 cm/s); (b) geostrophic velocity (contour interval 0.05 m/s) , (c) Ekman velocity (contour interval 0.05 m/s), and (d) Stokes velocity (contour interval 0.01 m/s).

In the model, floats were released in a $4^\circ \times 4^\circ$ domain on January 1st, 2008. Figure 3.2 a shows their trajectories for the time period of one year. The floats to

the north of the Labrador coast and to the east of Greenland launched in cold waters (blue) tend to quickly converge towards the boundary current and then follow the boundary current "highway". Indeed, the pattern of the surface Ekman velocity (Figure 3.1c) in these two regions is such that it carries the floats towards the boundary current where they are picked up by the quasigeostrophic velocity.

In contrast, the floats released in the Atlantic ocean south of Iceland (green) move quite chaotically and tend to linger in this area which is characterized by strong mesoscale variability. In addition, the total surface velocity is relatively weak in the central part of this region (Figure 3.1a) which also contributes to the observed behavior of the floats.

The surface temperature shows the most significant horizontal gradients in the southern part of the region (see Figure 2.2). The Labrador current brings cold and fresh waters along the coast of Newfoundland. The North Atlantic Current (NAC) transports warm and salty waters of subtropical origin northeastward into the eastern Subpolar North Atlantic. Most of the floats released in the warm southern part of the model region (red) move quickly along the NAC path. The baroclinic instability generates an intense mesoscale variability in the NAC (see Figure 3.1b). The related eddy-induced transport brings some of the floats released in the NAC into the central part of the Subpolar Gyre.

Figure 3.2b shows the components of velocity averaged over the entire ensemble of floats. In addition, all three time series are low-pass filtered with a running 5-day window. The Ekman and Stokes components (green and blue respectively) demonstrate clear seasonal variability having larger magnitude in the winter and fall seasons (days 1-100 and 250-365). It is not surprising since both of them are driven by wind.

Unfiltered time series (not shown here) show high-frequency variations with a period of 2-3 days during strong storms. The magnitude of these events are several times higher than the mean values. The seasonal cycle is less pronounced in the quasi-geostrophic velocity component (red) which remains relatively flat during winter and spring, slightly decreases in the summer and somewhat increases in the fall.

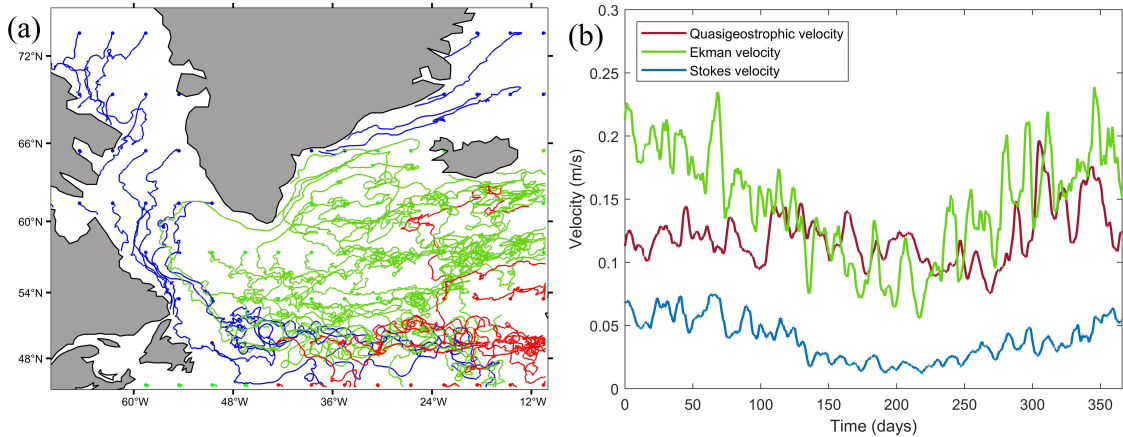


Figure 3.2: Surface float trajectories (a) and velocity components (b). Trajectories are colored according to the annual mean sea surface temperature at the point of release: $t > 16^\circ\text{C}$ (red), $3^\circ\text{C} < t < 16^\circ\text{C}$ (green) and $t < 3^\circ\text{C}$ (blue). Quasigeostrophic (red line), Ekman (green line) and Stokes (blue line) components of velocity are averaged over the entire ensemble of floats.

3.2 Icebergs

In contrast to floats, which are carried passively by surface currents, icebergs are directly exposed to wind above the surface of water as well as to currents in the

deeper layers below the surface. As a result, their dynamics is more diverse. Different forcing terms in the momentum equation (1.1) affect iceberg trajectories to a different degree. Smaller icebergs can be compared with a sailboat which is driven by wind and ocean currents; the dominant forces are form drags due to motion of air and water [6]. For larger icebergs, the combined Coriolis and pressure gradient force becomes significant [35]. In our model, the forcing is derived from eddy-resolving ocean data and high-frequency 1-hour surface forcing. This allows us to study how the balance of forces varies along iceberg trajectories for different categories of icebergs.

Figure 3.3 shows trajectories of 16 icebergs of each category (6 categories out of 8 are shown, Table 2.1). The icebergs are released in a small area offshore the Jakobshavn Glacier. Their trajectories then follow the cyclonic circulation in the Labrador Sea staying tightly within the boundary current. In this respect, the iceberg trajectories are generally similar to those of surface floats (Figure 3.2 a). However, there are essential differences as well. In contrast to floats, icebergs tend to linger close to the area where they were released for a relatively long period of time of approximately 3 months. Smaller icebergs remain in this area longer; the smallest of them melt there and never advance very far (Figure 3.3a). Larger icebergs, however, make their way to the Labrador current and are carried all the way out of the Labrador Sea to the open ocean.

To further understand how the forces applied on icebergs vary during different weather events we plot their magnitude as a function of time for each cluster of icebergs (Figure 3.4). Only the first 120 days of iceberg voyage are shown. Figure 3.4 shows that all forces exhibit variations related to passing weather disturbances over the region. Note that the time series in Figure 3.4 were filtered with a low-pass filter

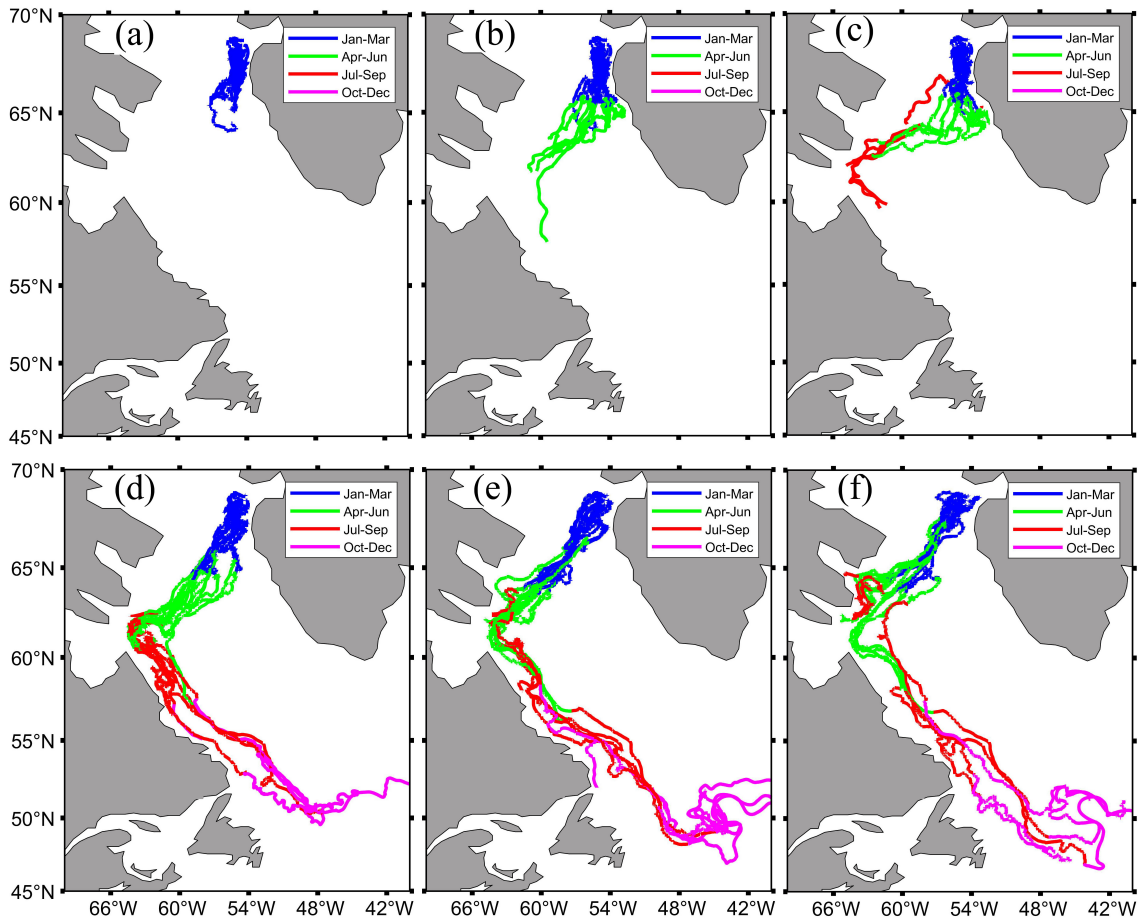


Figure 3.3: Trajectories of icebergs of different mass: categories 3 (a), 4 (b), 5 (c), 7 (d), 9 (e) and 10 (f) (Table 2.1)

with running 5-day window. Original data (not shown here) exhibit variability of even higher frequency. During a storm the air drag increases rapidly in magnitude over a period of a several hours to one day. As a result, icebergs accelerate; the degree of acceleration can be deduced from the magnitude of the net force (black line). Increased iceberg velocity with respect to water causes the increase of the water drag such that air and water drags become well balanced ("sailboat" behaviour). Since the air and water drag cancel each other almost completely the combined Coriolis and pressure gradient force is the one that determine the net force on the iceberg (Figure 3.4a).

Almost identical variation of air and water drag is exhibited by smaller icebergs Figure 3.4a, b while for larger icebergs Figure 3.4e, f the combined Coriolis and pressure gradient force follows the air drag quite closely. The main reason that the balance of forces depends on the iceberg size is that the drag forces (1.2) and the combined Coriolis and pressure gradient force (1.5) scale differently with size. Drag forces are proportional to cross-sectional areas (either under or above water) which both scale as length squared. The combined Coriolis and pressure gradient force, \vec{F}_{Cp} , on the other hand, is proportional to mass and scales as length cubed. Thus, \vec{F}_{Cp} becomes more dominant for larger icebergs. Another consequence of the balance shift is that the water drag becomes relatively small. Since the water drag is proportional to the difference between the ocean current velocity and iceberg velocity, this indicates that these velocities are close. In other words, very large icebergs are carried mostly by ocean current. Note, however, that the largest categories of icebergs are more typical for those observed in Antarctica rather than in the Arctic.

Consider the evolution of forces during a single storm passing over the Western

North Atlantic on days 41-46. Vector diagrams in Figure 3.5 show the time series of forces for four icebergs of different mass. For smaller icebergs (Figure 3.5a, b) the air and water drag forces are of opposite direction and of the same amplitude; they are in almost perfect balance. The combined Coriolis and pressure gradient force is much smaller; together with the residual of the balanced stronger drag forces it results in the net force.

Forces are quite different for larger icebergs both in direction and magnitude (Figure 3.5 c, d). During the strongest wind on days 43 - 44, the air drag becomes very large. The water drag also increases significantly during this period and together with the combined Coriolis and pressure gradient force balances the air drag. Overall balance is achieved between these three forces. The resultant net force is relatively small compared to the individual components. It is also interesting to observe what happens when winds are light (days 41 - 42) or moderate (days 45 - 46). The water drag becomes negligible while the air drag and the combined Coriolis and pressure gradient force cancel each other almost exactly.

It is instructive to compare the direction of iceberg velocity with that of wind and water velocity. Figure 3.6 shows vector diagrams of velocity during the same days as the force diagrams in Figure 3.5. Remarkably, the iceberg velocity is very well aligned with the wind for smaller icebergs (Figure 3.6a, b), the icebergs drift downwind. This is in agreement with [13], [?] as well as with the results of the analytical model by *Wagner et al.*. In contrast, larger icebergs drift at an angle of approximately 45 deg to the right of the wind during strong winds and at approximately 90 deg angle during light winds. The latter result is in agreement with the model by *Wagner et al.* where it occurred in an asymptotic case of large icebergs and light winds. Further

comparing iceberg velocities with the surface velocity of seawater one can see that they are quite different both in direction and magnitude for all icebergs. Since the surface velocity is the one carrying the surface floats, it is clear that icebergs drift differently.

Icebergs melt during their journey delivering cold fresh water to the environment. The amount of fresh water depends on how long an iceberg stays in a particular area as well as on the control parameters in equations (1.9, 1.13, 1.14). Perhaps the main parameter affecting the melting rate is the seawater temperature, T_w . Figure ??c shows that seawater becomes warmer by approximately 2-3 C along a typical iceberg trajectory following the boundary current from offshore the Jakobshavn Glacier to the end of the Labrador coast. Beyond that, seawater temperature increases rapidly in the eastern direction towards the warm waters of the North Atlantic Current. Figure 3.7 shows the simulated amount of freshwater delivered by icebergs. This amount is averaged over an area of $0.5^\circ \times 0.5^\circ$ and shown in cm. A pattern of melting is similar for all icebergs, although larger icebergs deliver more freshwater, as one might expect. Maximum amount of fresh water is delivered in the area west of Greenland where icebergs spend longer time. Similar melting patterns were reported in the previous simulations by different authors [?, 35].

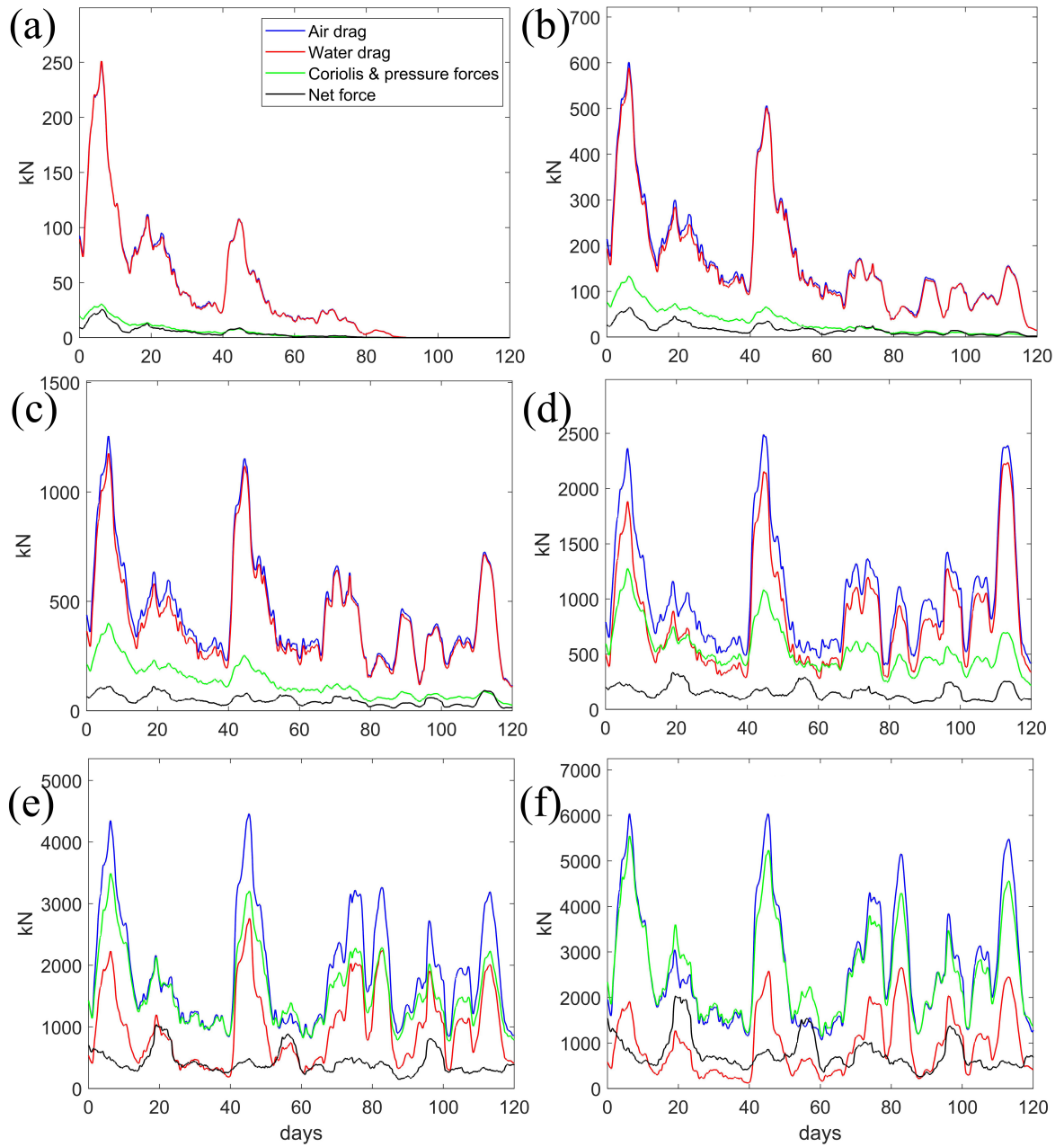


Figure 3.4: The magnitude of forces applied on icebergs of different mass during the first 120 days of their journey: categories 3 (a), 4 (b), 5 (c), 7 (d), 9 (e) and 10 (f) (Table 2.1)

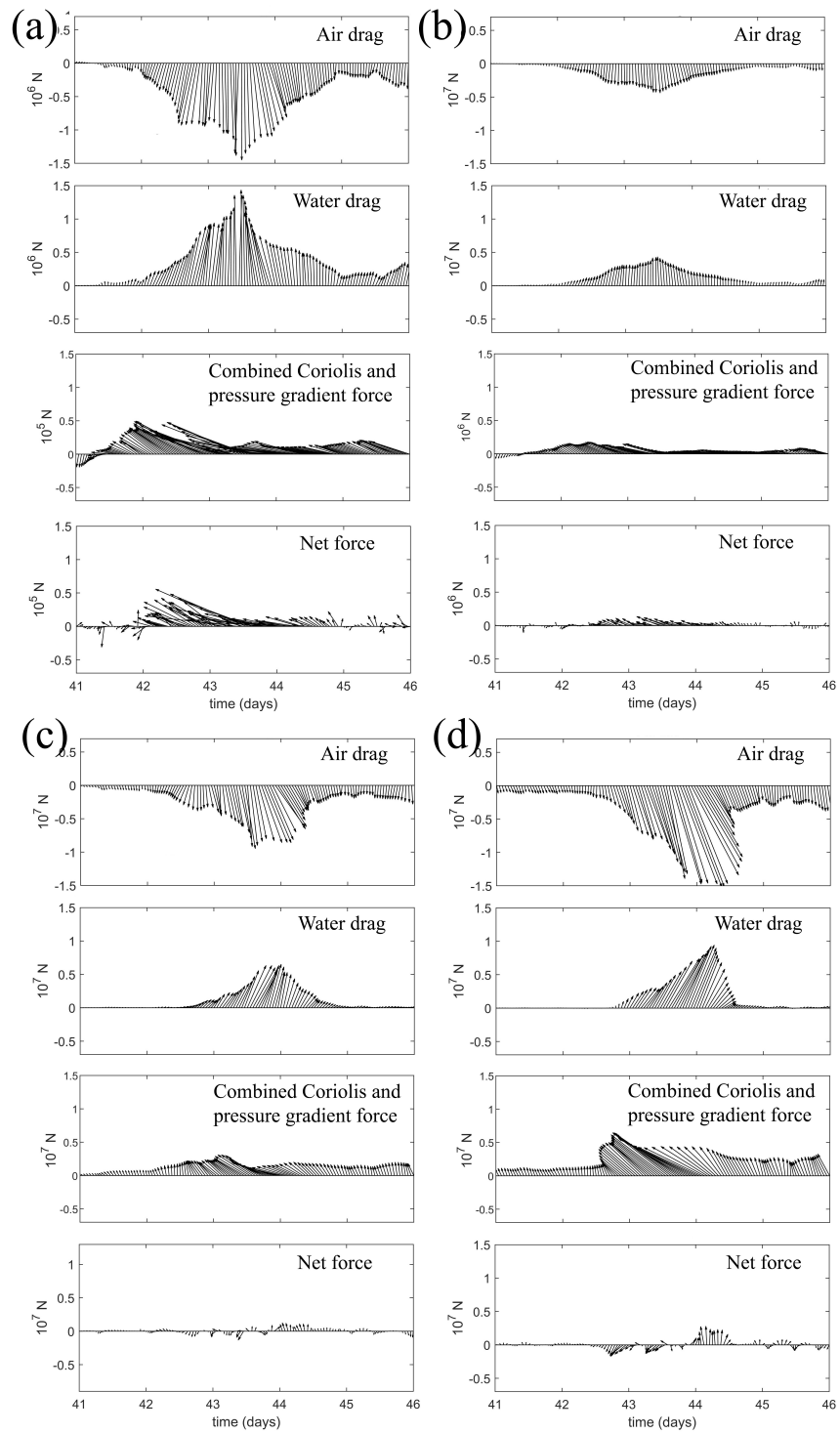


Figure 3.5: Vector diagrams of forces for icebergs of different masses during a storm event: categories 4 (a), 5 (b), 9 (c) and 10 (d) (Table 2.1).

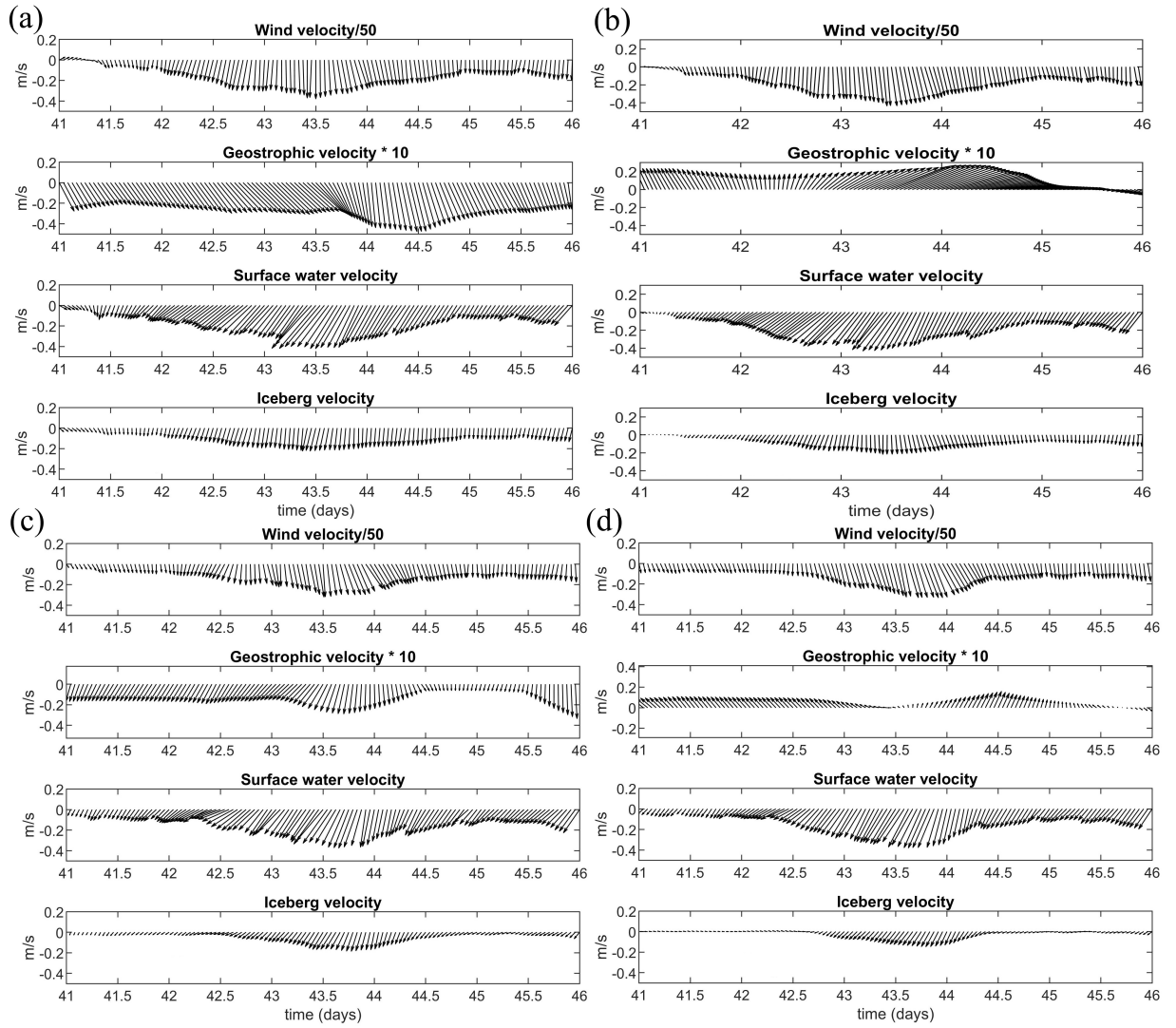


Figure 3.6: Vector diagrams of air, water and iceberg velocity for icebergs of different mass during a storm event: categories 4 (a), 5 (b), 9 (c) and 10 (d) (Table 2.1).

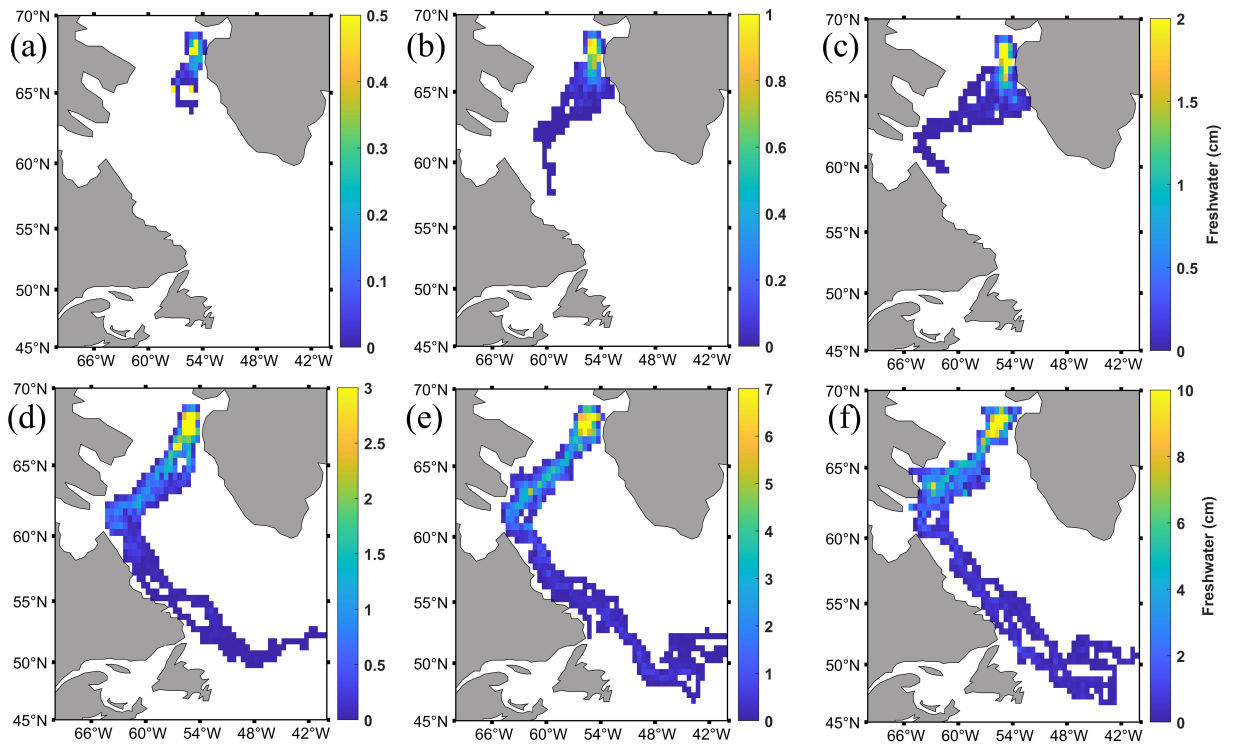


Figure 3.7: Intensity of melting along the iceberg paths: categories 3 (a), 4 (b), 5 (c), 7 (d), 9 (e) and 10 (f) (Table 2.1)

Chapter 4

Conclusions

This study described an idealized model of iceberg drift. The momentum equation of the model contains environmental forcing terms including air and water drag and the combined Coriolis and pressure gradient force. The model requires input data, which can be obtained by remote measurements. In particular, seawater velocity can be computed using altimetry data, but it is not limited to geostrophy as it also includes higher-order terms due to non-linearity and time tendency. The measured characteristics of wind and surface waves allow us to compute the Ekman and Stokes components of velocity. It should be noted that the latter two components are depth dependent, and analytical equations are used to describe their vertical variation. Presently, we use sea surface height from a reanalysis model, but in the future high-resolution satellite altimetry data can be used directly.

Simulated surface floats and iceberg trajectories in the Labrador Sea for the year 2008. Both floats and icebergs that start their journey west of the coast of Greenland converge into the Labrador Current and are carried into the North Atlantic. Floats

that are assumed to be passive Lagrangian tracers are carried by the surface velocity. The dominant component of the velocity is the Ekman component, especially during strong winds. The quasigeostrophic velocity, which is a sum of the geostrophic, non-linear and time tendency components, is a close second.

Air and water drag and the combined Coriolis and pressure gradient forces exerted on icebergs show high variability at a synoptic time scale. This variability is driven by atmospheric disturbances passing over the Labrador Sea. Strong winds directly affect the air drag, while the water drag is affected via the Ekman component of water velocity. While the duration of strong atmospheric disturbances is typically limited to a few days, the resulting forces on the iceberg can rise significantly compared to their magnitude outside the storm periods.

Both similarities as well as significant differences with the analytical model by *Wagner et al* were observed, especially during passing storms when the iceberg motion is not steady-state as assumed by the analytical model. In addition, the balance of forces varies during these events.

Future simulations of iceberg trajectories should consider using sub-mesoscale ocean data with the goal of investigating the sensitivity of the trajectories to such "less smooth" forcing. These data can be provided by a high-resolution regional ocean model embedded in a global model.

Bibliography

- [1] Y. D. Afanasyev. Altimetry in a GFD laboratory and flows on the polar β -plane. In T. von Larcher and P. Williams, editors, *Modelling Atmospheric and Oceanic Flows: Insights from Laboratory Experiments and Numerical Simulations*, chapter 5, pages 101–117. AGU Wiley, Hoboken, New Jersey, 2015.
- [2] Y. D. Afanasyev. Turbulence, Rossby waves and zonal jets on the polar β -plane: Experiments with laboratory altimetry. In B. Galperin and P. L. Read, editors, *Zonal jets: Phenomenology, genesis, and physics*, chapter 8, pages 152–166. Cambridge Univ. Press, New York, 2019.
- [3] Y. D. Afanasyev, S. O’Leary, P. B. Rhines, and E. G. Lindahl. On the origin of jets in the ocean. *Geoph. Astroph. Fluid Dyn.*, 106:113–137, 2012.
- [4] Y. D. Afanasyev, P. B. Rhines, and E. G. Lindahl. Velocity and potential vorticity fields measured by altimetric imaging velocimetry in the rotating fluid. *Exp. Fluids*, 47:913–926, 2009.
- [5] G. Bigg and S. Billings. The iceberg risk in the titanic year of 1912: Was it exceptional? *Significance*, 11(3):6–10, 2014.

- [6] G. R. Bigg, M. R. Wadley, D. P. Stevens, and J. A. Johnson. Prediction of iceberg trajectories for the north atlantic and arctic oceans. *Geophysical research letters*, 23(24):3587–3590, 1996.
- [7] G. R. Bigg, M. R. Wadley, D. P. Stevens, and J. A. Johnson. Modelling the dynamics and thermodynamics of icebergs. *Cold Regions Science and Technology*, 26(2):113–135, 1997.
- [8] J. E. Box, A. Hubbard, D. B. Bahr, W. T. Colgan, X. Fettweis, K. D. Mankoff, A. Wehrlé, B. Noël, M. R. van den Broeke, B. Wouters, et al. Greenland ice sheet climate disequilibrium and committed sea-level rise. *Nature Climate Change*, pages 1–6, 2022.
- [9] G. P. Compo, J. S. Whitaker, P. D. Sardeshmukh, N. Matsui, R. J. Allan, X. Yin, B. E. Gleason, R. S. Vose, G. Rutledge, P. Bessemoulin, et al. The twentieth century reanalysis project. *Quarterly Journal of the Royal Meteorological Society*, 137(654):1–28, 2011.
- [10] B. Cushman-Roisin, E. P. Chassignet, and B. Tang. Westward motion of mesoscale eddies. *Journal of Physical Oceanography*, 20:758–768, 1990.
- [11] D. Dobhal and M. Mehta. Shrinking himalayan glaciers and their impact on environment.
- [12] V. W. Ekman. On the influence of the earth’s rotation on ocean-currents. *Almqvist & Wiksells boktryckeri, A.-B.*, 1905.

- [13] C. Garrett, J. Middleton, M. Hazen, and F. Majaess. Tidal currents and eddy statistics from iceberg trajectories off labrador. *Science*, 227(4692):1333–1335, 1985.
- [14] R. Gladstone, G. Bigg, and K. Nicholls. Icebergs and fresh water fluxes in the southern ocean. *J. Geophys. Res*, 106:19903–19915, 2001.
- [15] R. M. Gladstone, G. R. Bigg, and K. W. Nicholls. Iceberg trajectory modeling and meltwater injection in the southern ocean. *Journal of Geophysical Research: Oceans*, 106(C9):19903–19915, 2001.
- [16] E. Hanna, S. H. Mernild, J. Cappelen, and K. Steffen. Recent warming in greenland in a long-term instrumental (1881–2012) climatic context: I. evaluation of surface air temperature records. *Environmental Research Letters*, 7(4):045404, 2012.
- [17] H. Hersbach, B. Bell, P. Berrisford, A. Biavati, G. and Horányi, J. Muñoz Sabater, J. Nicolas, C. Peubey, R. Radu, I. Rozum, D. Schepers, A. Simmons, C. Soci, D. Dee, and J.-N. Thépaut. Era5 hourly data on single levels from 1979 to present. *Copernicus Climate Change Service*, 2018.
- [18] D. M. Holland, R. H. Thomas, B. De Young, M. H. Ribergaard, and B. Lyberth. Acceleration of Jakobshavn Isbræ triggered by warm subsurface ocean waters. *Nature Geoscience*, 1(10):659–664, Oct. 2008.
- [19] Z. Hui and Y. Xu. The impact of wave-induced coriolis-stokes forcing on satellite-derived ocean surface currents. *Journal of Geophysical Research: Oceans*, 121(1):410–426, 2016.

- [20] T. H. Jacka and A. B. Giles. Antarctic iceberg distribution and dissolution from ship-based observations. *Journal of Glaciology*, 53(182):341–356, 2007.
- [21] I. Keghouche, F. Counillon, and L. Bertino. Modeling dynamics and thermodynamics of icebergs in the barents sea from 1987 to 2005. *Journal of Geophysical Research: Oceans*, 115(C12), 2010.
- [22] B. Liu, K. Wu, and C. Guan. Global estimates of wind energy input to subinertial motions in the ekman-stokes layer. *J. Oceanogr.*, 63(3):457–466, 2007.
- [23] T. Martin and A. Adcroft. Parameterizing the fresh-water flux from land ice to ocean with interactive icebergs in a coupled climate model. *Ocean Modelling*, 34(3-4):111–124, 2010.
- [24] A. M. Matulka, Y. Zhang, and Y. D. Afanasyev. Complex environmental β -plane turbulence: laboratory experiments with altimetric imaging velocimetry. *Nonlinear Processes in Geophysics*, 23(1):21–29, 2016.
- [25] D. L. Murphy and J. L. Cass. The international ice patrol: safeguarding life and property at sea. *Coast Guard Journal of Safety & Security at Sea, Proceedings of the Marine Safety & Security Council*, 69(2), 2012.
- [26] J. Parayil, E. Demirov, and Y. D. Afanasyev. Effects of wind, waves, and currents on icebergs and surface floats in the labrador sea: A modeling study. *Journal of Marine Science and Engineering*, 10(9):1167, 2022.
- [27] O. M. Philipps. The dynamics of the upper ocean. *Cambridge Univ. Press*, 1977.

- [28] J. A. Polton, D. M. Lewis, and S. E. Belcher. The role of wave-induced coriolis–stokes forcing on the wind-driven mixed layer. *Journal of Physical Oceanography*, 35(4):444–457, 2005.
- [29] Y. A. Romanov, N. A. Romanova, and P. Romanov. Distribution of icebergs in the atlantic and indian ocean sectors of the antarctic region and its possible links with enso. *Geophysical research letters*, 35(2), 2008.
- [30] F. Santiago-Mandujano and E. Firing. Mixed-layer shear generated by wind stress in the central equatorial pacific. *Journal of Physical Oceanography*, 20(10):1576–1582, 1990.
- [31] T. Silva, G. Bigg, and K. Nicholls. Contribution of giant icebergs to the southern ocean freshwater flux. *Journal of Geophysical Research: Oceans*, 111(C3), 2006.
- [32] T. A. M. d. Silva. *Quantifying Antarctic icebergs and their melting in the ocean*. PhD thesis, University of Sheffield, 2006.
- [33] K. Stuart and D. Long. Tracking large tabular icebergs using the seawinds ku-band microwave scatterometer. *Deep Sea Research Part II: Topical Studies in Oceanography*, 58(11-12):1285–1300, 2011.
- [34] I. Team. Mass balance of the greenland ice sheet from 1992 to 2018. *Nature*, 579:233–239, 2020.
- [35] T. J. Wagner, R. W. Dell, and I. Eisenman. An analytical model of iceberg drift. *Journal of Physical Oceanography*, 47(7):1605–1616, 2017.
- [36] R. White. The proposed strait of belle isle cable crossing. *Proto-Type*, 1, 2013.

- [37] D. J. Wilton, G. R. Bigg, and E. Hanna. Modelling twentieth century global ocean circulation and iceberg flux at 48 n: implications for west greenland iceberg discharge. *Progress in Oceanography*, 138:194–210, 2015.
- [38] K. Wu and B. Liu. Stokes drift-induced and direct wind energy inputs into the ekman layer within the antarctic circumpolar current. *Journal of Geophysical Research: Oceans*, 113(C10), 2008.
- [39] Y. Zhang and Y. Afanasyev. Beta-plane turbulence: Experiments with altimetry. *Phys. Fluids*, 26:026602, 2014.
- [40] Y. Zhang and Y. Afanasyev. Baroclinic turbulence on the polar beta-plane in the rotating tank: Down to submesoscale. *Ocean Modelling*, 107:151–160, 2016.